National School on Neutron and X-Ray Scattering

Argonne and Oak Ridge National Laboratories

Polarized Neutrons

24 June 2014

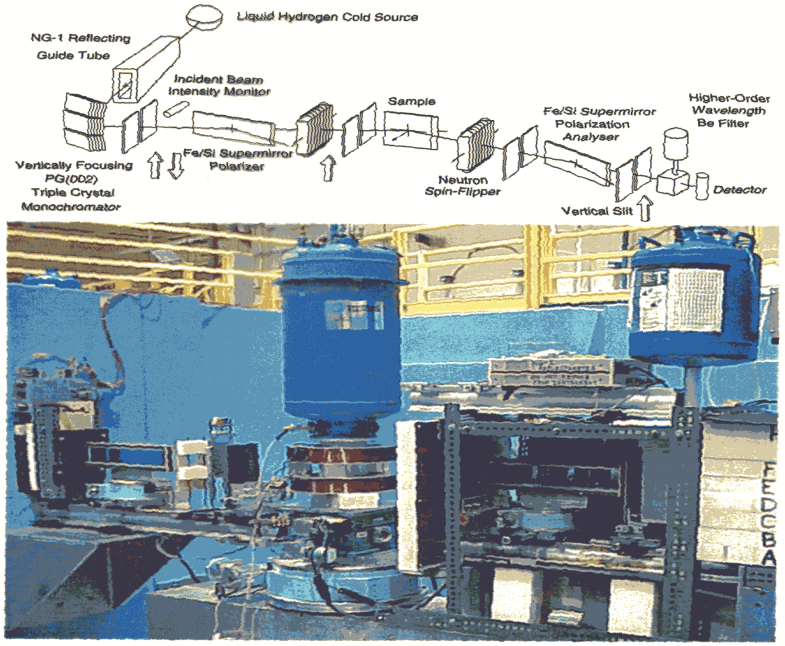

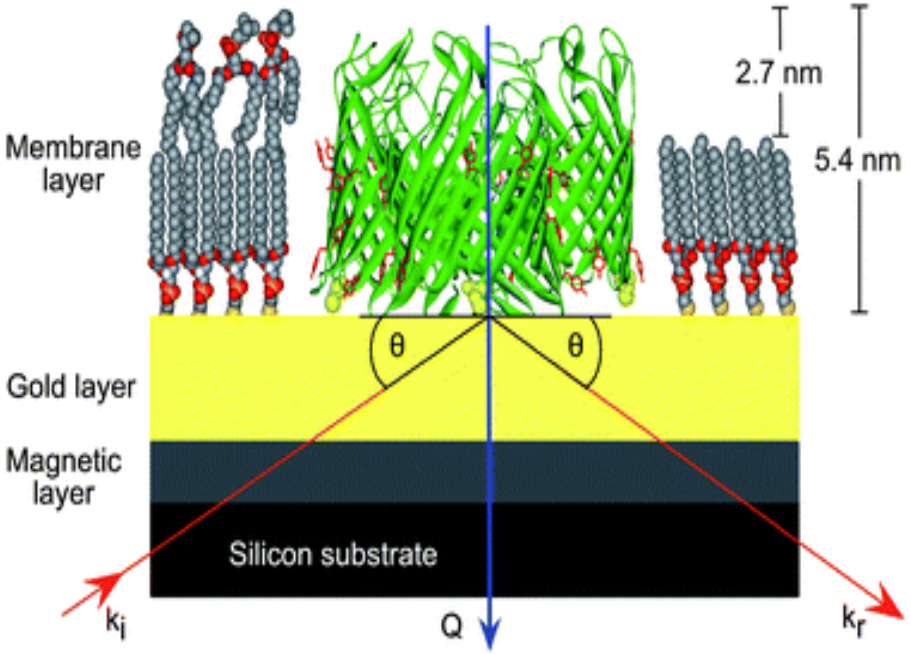

C.F.Majkrzak, *NIST Center for Neutron Research*,
Gaithersburg, MD

Part 1: Neutron polarization -- fundamental concepts

Part 2: Brief discussion of the application of polarized neutrons in the study of the magnetic structures of hard condensed matter

Part 3: Application of polarized neutrons and ferromagnetic reference layers to phase-sensitive neutron reflectometry studies of the structure of soft condensed matter systems

Part 4: Application of polarized neutrons in measurements of very small energy and momentum transfers with condensed matter systems

Part 1: Neutron polarization -- fundamental concepts

<> a magnetic moment arises from the motion of electrical charges -- though neutral, a neutron is composed of charged quarks which give rise to a net magnetic dipole moment which is quantized with corresponding spin 1/2 -- a neutron is a Fermion

<> if it exists at all, any neutron electric dipole moment is of negligible magnitude for all practical purposes of concern to us here

<> a neutron can be represented by a spinor wave function having two components corresponding to two spin eigen-states (spin “+” or “up” and “-” or “down”)

<> for a nucleus with spin, the neutron-nucleus (i.e., the *nuclear*) interaction is spin-dependent

<> the *magnetic* interaction between the neutron magnetic moment and that of a *nuclear* magnetic moment is relatively weak (and nuclear magnetic moments are normally not ordered -- a notable exception occurring in a 3He gas cell used as a neutron polarizer)

<> the *magnetic* interaction between the neutron magnetic moment and that of an atomic magnetic moment, on the other hand, can be comparable to the nuclear interaction

(a good description of the phenomenon of a quantized spin one-half system is given in the quantum mechanics text by Merzbacher)

$$\Psi = \psi_+ + \psi_- = \underbrace{C_{0_+} e^{i\vec{k}_+\cdot\vec{r}} \begin{pmatrix} 1 \\ 0 \end{pmatrix}}_{C_+} + \underbrace{C_{0_-} e^{i\vec{k}_-\cdot\vec{r}} \begin{pmatrix} 0 \\ 1 \end{pmatrix}}_{C_-}$$

$$k_\pm = n_\pm k_0$$

$$n_\pm^2 = 1 - \frac{2m}{(\hbar k_0)^2}\left(V_N \pm \mu B\right)$$

$$= 1 - \frac{4\pi}{k_0^2}\left(\rho_N \pm \rho_M\right)$$

NUCLEAR SLD

MAGNETIC SLD

$$|\Psi|^2 = \Psi^{*T}\Psi = \left(\psi_+^* \psi_-^*\right)\begin{pmatrix} \psi_+ \\ \psi_- \end{pmatrix}$$

$$= \psi_+^*\psi_+ + \psi_-^*\psi_-$$

$$= C_{0_+}^* e^{-i\vec{k}_+\cdot\vec{r}} C_{0_+} e^{+i\vec{k}_+\cdot\vec{r}} + C_{0_-}^* e^{-i\vec{k}_-\cdot\vec{r}} C_{0_-} e^{+i\vec{k}_-\cdot\vec{r}}$$

$$= |C_{0_+}|^2 + |C_{0_-}|^2 = 1$$

The neutron is a spin-half quantum object and possesses a corresponding magnetic moment. Its wave function must therefore be described as a "spinor" which is composed of two terms, each representing one of two possible spin "eigenstates". In a magnetic field, the energies associated these two eigenstates are different. This can have significant consequences for the interaction of the neutron with magnetic fields and materials.

So our description of a neutron gets a bit more complicated when we have to take into account its spin and moment. But, as I hope you will see, that added complexity makes the neutron a more sensitive and useful probe of matter, even that which is not itself magnetic.

The magnetic SLD is a product of the number of magnetic atoms per unit volume times their characteristic magnetic scattering length (usually designated "p") -- *or* is proportional to a macroscopic magnetic induction field "B".

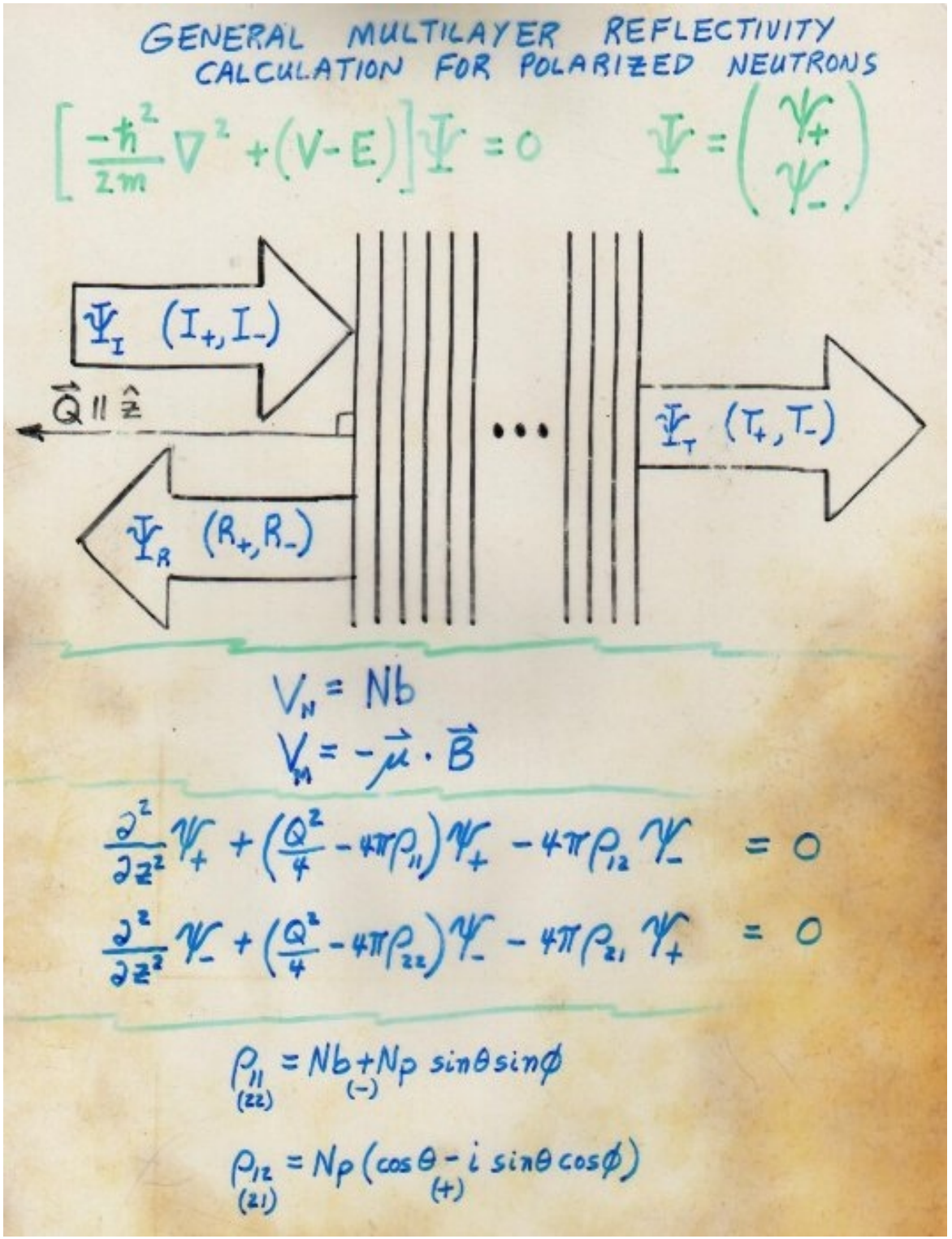

For polarized neutrons, solving the Schroedinger equation of motion -- say for specular reflection, as we have done previously in the absence of magnetic fields -- now requires a simultaneous solution of a pair of coupled equations. This takes into account the possibility that a scattering event or interaction will involve a change in the neutron's spin eigenstate from “+” or “up” to “-” or “down” (or not). Note that the nuclear and magnetic SLDs or potentials are additive and thus result in an interference in some cases that is neutron spin-dependent.

$$\underline{V_M} = -\underline{\mu} \cdot \vec{B}$$

$$= -\gamma_m \left\{ \underline{S_x} B_x + \underline{S_y} B_y + \underline{S_z} B_z \right\}$$

$$= -\gamma_m \frac{\hbar}{2} \left\{ \begin{pmatrix} 0 & B_x \\ B_x & 0 \end{pmatrix} + \begin{pmatrix} 0 & -iB_y \\ iB_y & 0 \end{pmatrix} + \begin{pmatrix} B_z & 0 \\ 0 & -B_z \end{pmatrix} \right\}$$

$$= -\gamma_m \frac{\hbar}{2} \begin{pmatrix} B_z & B_x - iB_y \\ B_x + iB_y & -B_z \end{pmatrix}$$

$$= \frac{h^2}{2m\pi} \begin{pmatrix} N\rho_z & N\rho_x - iN\rho_y \\ N\rho_x + iN\rho_y & -N\rho_z \end{pmatrix}$$

- ONLY COMPONENTS OF $\vec{B} \perp \vec{Q}$ ARE EFFECTIVE IN SCATTERING NEUTRONS

$$\underline{\mu} = -\gamma_m \frac{\hbar}{2} \left\{ \begin{pmatrix} 0 & 1 \\ 1 & 0 \end{pmatrix} \hat{x} + \begin{pmatrix} 0 & -i \\ i & 0 \end{pmatrix} \hat{y} + \begin{pmatrix} 1 & 0 \\ 0 & -1 \end{pmatrix} \hat{z} \right\}$$

The potential energy or SLD can no longer be described as a scalar quantity but is, instead, represented by matrix -- the neutron moment itself is a vector operator composed of 2 x 2 so-called “Pauli” matrices.

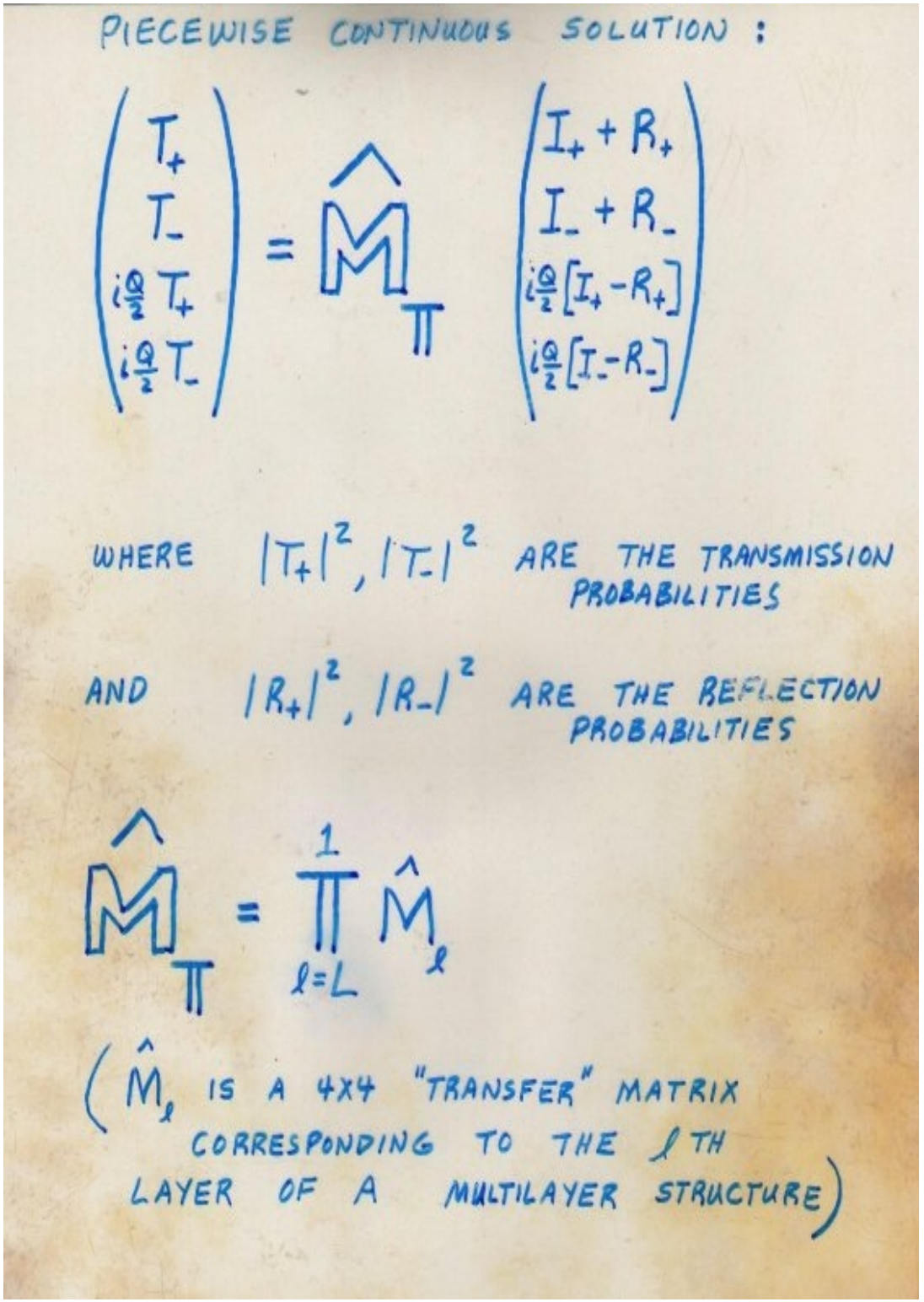

At the end of the day, we can arrive at a similar, but somewhat more complicated, relationship between transmitted (T_+ , T_-), reflected (R_+ , R_-), and incident (I_+ , I_-) wave amplitudes which are now spin-dependent. Just as we did for the non-polarized case, any arbitrary SLD profile can be rendered into slices of constant SLD (the “sliced-bread” analogy) for piece-wise continuous solution by imposing the boundary conditions of continuity on the wave function and its first derivative at each interface.

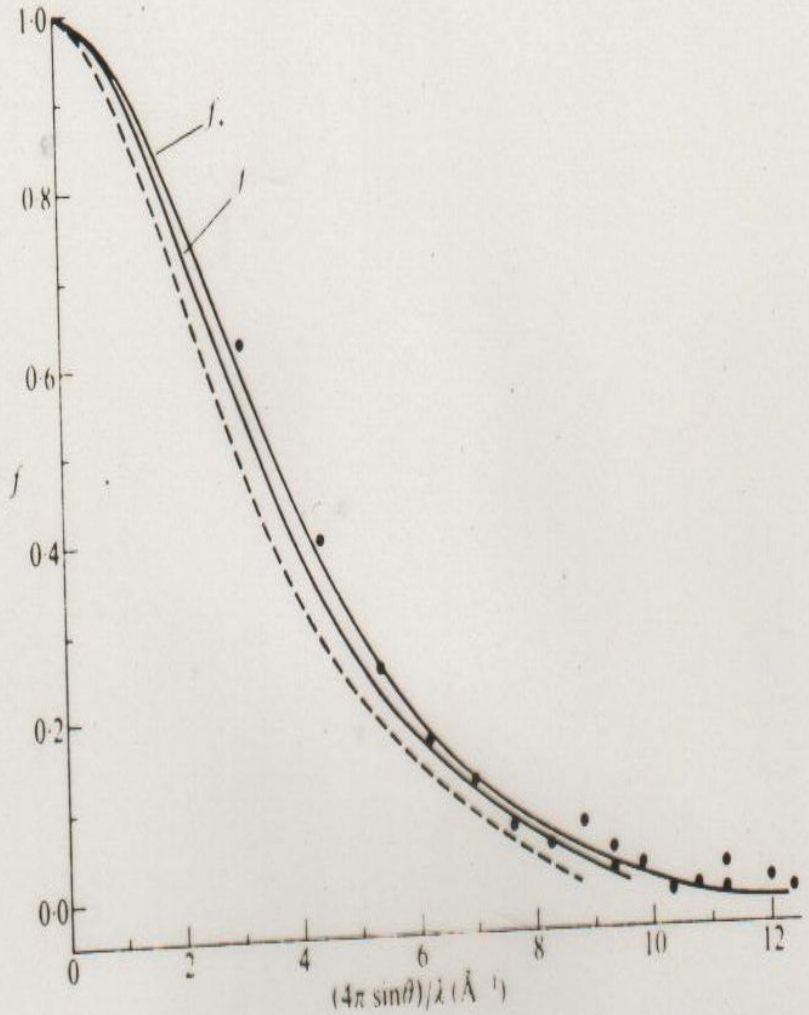

FIG. 126. Magnetic form factor curves for iron. The full-line curves show the calculation by Wood and Pratt for, respectively, the five 3d electrons of +ve spin and the single 3d electron of −ve spin for a free iron atom. The points are the experimental measurements of Shull and Yamada for metallic iron. The broken-line curve contrasts the experimental data for the Fe^{3+} ion in magnetite.

The atomic magnetic moments, with which the neutron magnetic moment interacts, originate from the atomic electrons with unpaired spins in the material. These electrons are relatively spread out in space in comparison to the nucleus which acts as a practical point in space as the source of the neutron's nuclear interaction. Consequently, the strength or magnitude of the corresponding magnetic scattering length “p” falls off with increasing scattering angle. Nonetheless, for scattering at low enough angle, such as in reflectometry or SANS, this variation can be negligible.

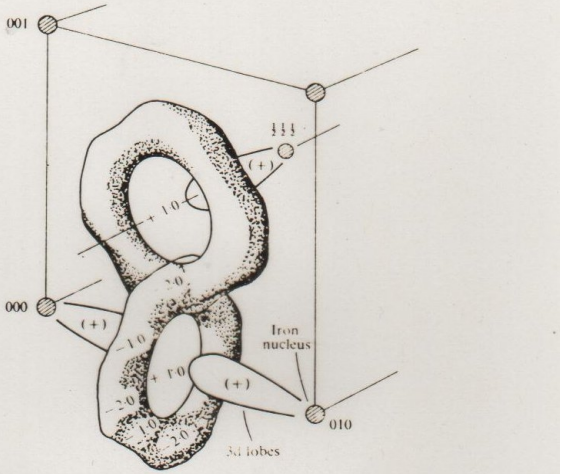

FIG. 134. The residual magnetization (kG) in iron as deduced experimentally by Shull and Mook (1966). The positive excess of 3d magnetization along the cube edges is over-emphasized in comparison with the interlocking rings of negative magnetization. The rings shown are centred on $0\frac{1}{2}0$, $0\frac{1}{2}\frac{1}{2}$.

Neutron Polarization Vector

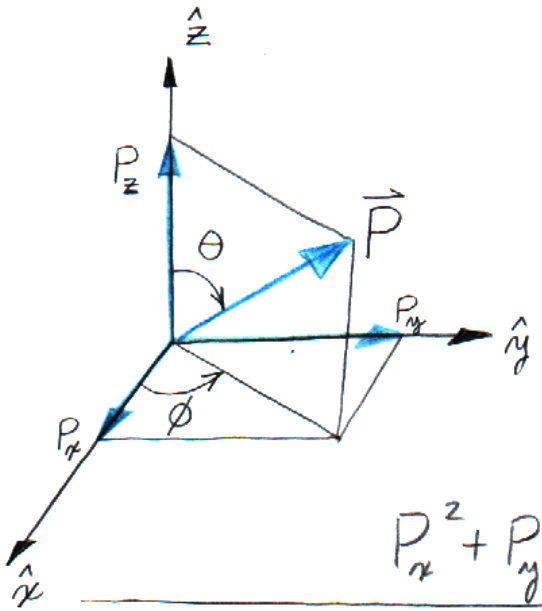

P_x	P_y	P_z	θ	ϕ	C_+	C_-
0	0	1	0	0	1	0
0	0	-1	π	0	0	1
1	0	0	$\pi/2$	0	$1/\sqrt{2}$	$1/\sqrt{2}$
0	1	0	$\pi/2$	$\pi/2$	$1/\sqrt{2}$	$i/\sqrt{2}$

$$\vec{P} = P_x\hat{x} + P_y\hat{y} + P_z\hat{z}$$

$$P_x^2 + P_y^2 + P_z^2 = 1$$

$$P_x = \sin\theta\cos\phi = 2\,\mathrm{Re}(C_+^* C_-)$$

$$P_y = \sin\theta\sin\phi = 2\,\mathrm{Im}(C_+^* C_-)$$

$$P_z = \cos\theta = |C_+|^2 - |C_-|^2$$

$$P_z = \frac{N_+ - N_-}{N_+ + N_-} \qquad |C_+|^2 = \frac{N_+}{N_+ + N_-} \qquad |C_-|^2 = \frac{N_-}{N_+ + N_-}$$

$$|C_+|^2 + |C_-|^2 = 1$$

$$C_+ = \cos\left(\frac{\theta}{2}\right)$$

$$C_- = \sin\left(\frac{\theta}{2}\right) e^{i\phi}$$

It is possible to mathematically construct a “polarization” vector **P** which describes some of the spin-dependent characteristics of an ensemble or collection of spin half neutrons composing a beam. The number of neutrons in the spin “+” or “-” eigenstates is N_+ or N_-, respectively. The coefficients C_+ and C_- of the spinor wave function for the neutron can be written in terms of these numbers and also can be related to the components of the polarization vector along the x-, y-, and z-directions. P can alternatively be described in terms of angles relative to the coordinate axes.

Polarization Rotation

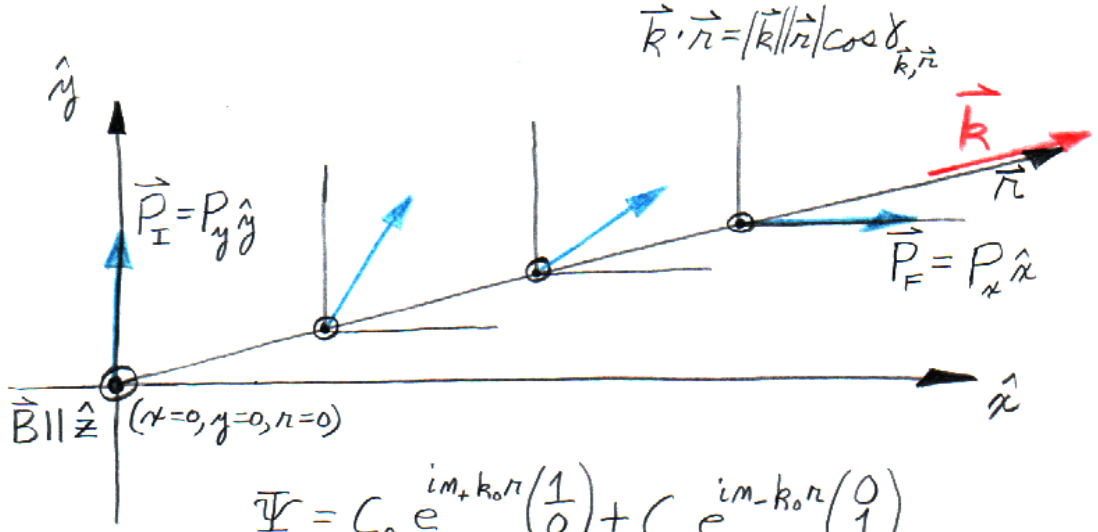

$$\Psi = \underbrace{C_{0+}e^{im_+k_0r}}_{C_+}\begin{pmatrix}1\\0\end{pmatrix} + \underbrace{C_{0-}e^{im_-k_0r}}_{C_-}\begin{pmatrix}0\\1\end{pmatrix}$$

$C_\pm = C_\pm(r)$ $\quad (\text{at } r=0,\ C_\pm = C_{0\pm})$

---

e.g.: $P_y(r) = 2\,\mathrm{Im}(C_+^* C_-)$

$$= 2\,\mathrm{Im}\left[C_{0+}^* e^{-im_+k_0r} C_{0-} e^{+im_-k_0r}\right]$$

$$= 2\,\mathrm{Im}\left[\left(\tfrac{1}{\sqrt{2}}\right)\left(\tfrac{i}{\sqrt{2}}\right)e^{i(m_- - m_+)k_0r}\right]$$

$$= \mathrm{Im}\left[i\cos\left([m_- - m_+]k_0r\right) - \sin\left([m_- - m_+]k_0r\right)\right]$$

$$\boxed{P_y(r) = \cos\left[(m_- - m_+)k_0r\right]} \qquad (P_y(r=0) = 1)$$

A net magnetic induction **B** defines an axis of quantization (conventionally taken to be parallel to the z-axis of a rectangular coordinate system or reference frame). Any component of the neutron polarization vector perpendicular to this **B** field will rotate with a characteristic "Larmor" frequency that is proportional to the difference between spin + and - refractive indices.

Precession of the Polarization

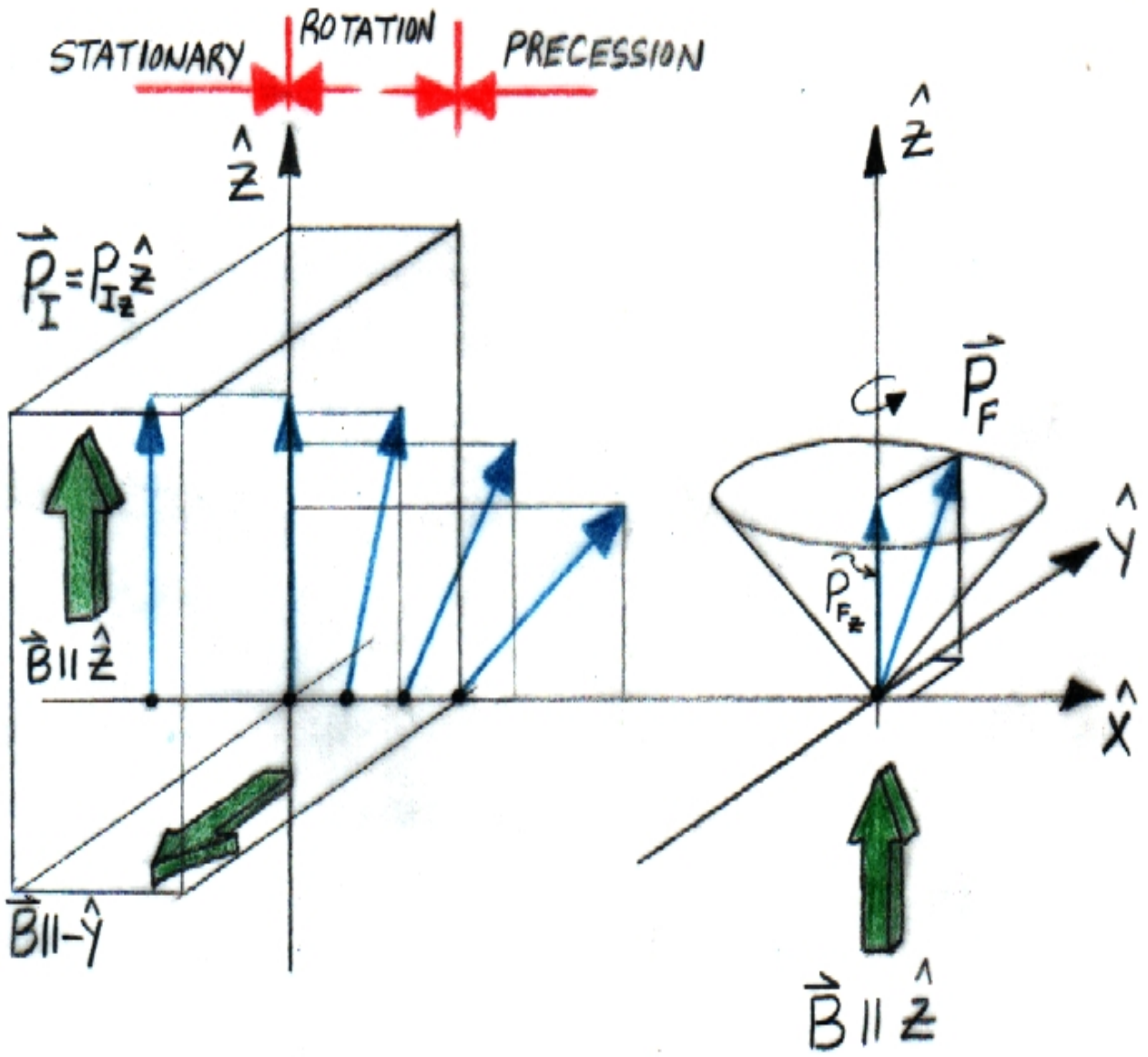

Precession is taken here to refer to a rotation of the polarization vector which persists through a given region of space other than for the purpose of effecting a reorientation of the polarization from one specific direction to another.

NEUTRON POLARIZER

5C

By reflection from a magnetic film with nuclear and magnetic scattering length densities such that $\rho_N - \rho_M = 0$ (for "−" spin state) and $\rho_N + \rho_M \neq 0$ (for "+" spin state).

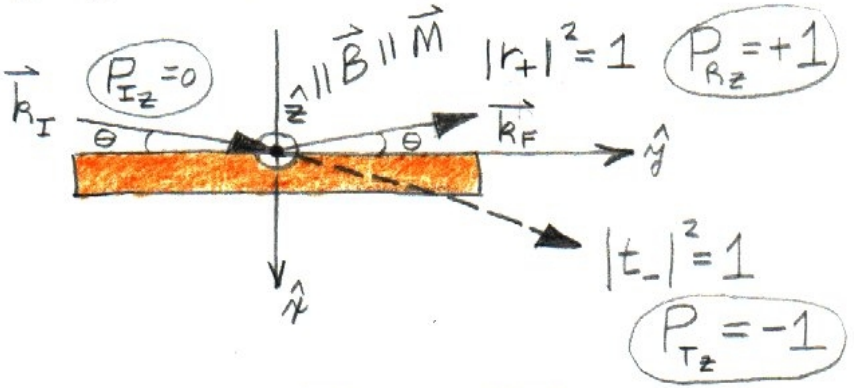

$|r_+|^2$

$(|r_-|^2 = 0,$

$|t_-|^2 = 1)$

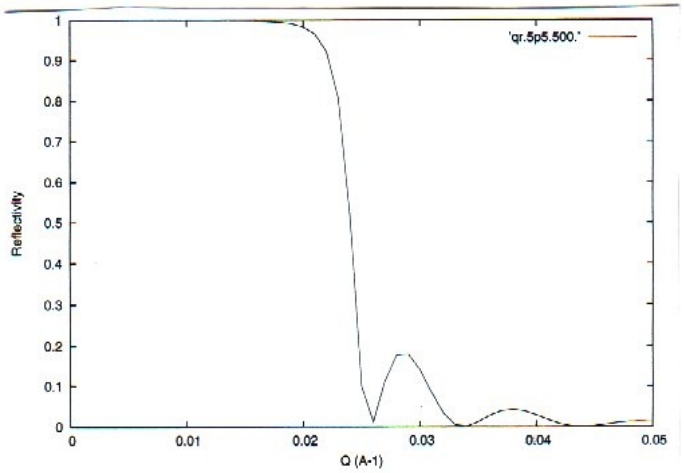

(CALCULATED USING FORMULAS OF FIGURE 3)

$Q = 2k_{0z} = 2k_0 \sin\theta$

$\rho_N + \rho_M = 10.0 \times 10^{-6}\ \text{Å}^{-2}$

$\rho_N - \rho_M = 0.0$ $\qquad L = 500.\ \text{Å}$

An unpolarized beam of neutrons can be polarized in a number of ways via interaction with a saturated ferromagnetic material. Perhaps the simplest involves specular reflection from a ferromagnetic plate with its magnetization saturated in the plane of the surface and normal to the wavevector transfer **Q**, as depicted in the figure to the left. Note that by matching the nuclear and magnetic SLDs of the material, one spin state will see a net interaction potential which is zero whereas the other will experience a net positive value. Consequently, one spin state is transmitted and the other reflected, thereby separating + and - neutrons in space.

Part 2: Brief discussion of the application of polarized neutrons in scattering studies of the structure of magnetic condensed matter

<> elastic scattering to determine magnetic *structures*

<> inelastic scattering to probe magnetic *excitations* such as spin waves

Much of what is known about the microscopic magnetic structure of materials has been obtained from neutron diffraction studies. These structures have been found to range from relatively simple ferromagnetic and anti-ferromagnetic alignments of atomic moments to far more complicated forms such as spin density waves and helices. Collective magnetic excitations in solids known as magnons or spin waves are studied by neutron inelastic scattering. Although these magnetic structures are primarily found in hard condensed matter, it is instructive to briefly consider the interaction of polarized neutrons with such materials prior to considering specific applications of polarized neutron in scattering studies of non-magnetic soft matter.

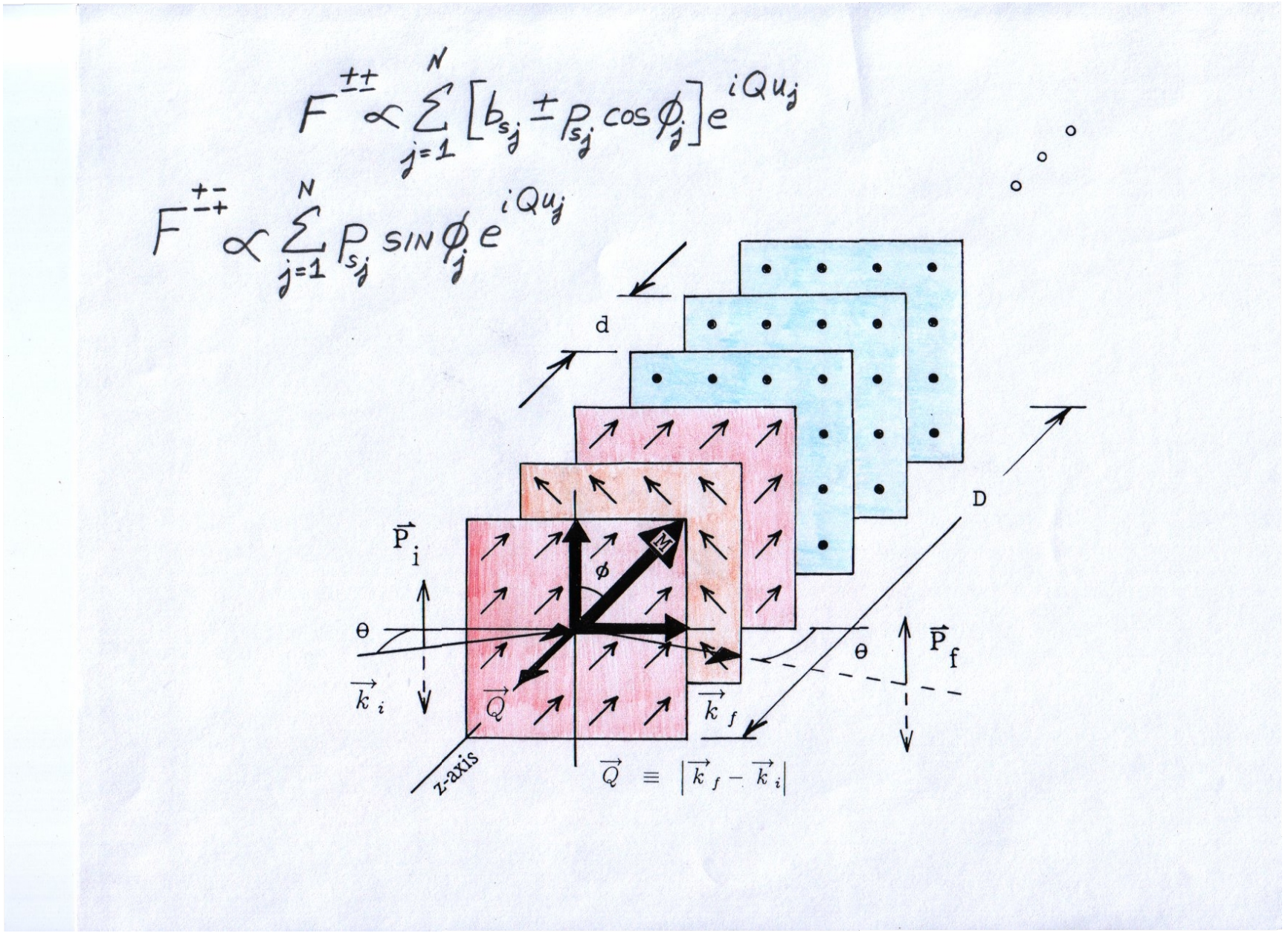

The above diagram illustrates a particularly useful configuration resulting in the ability to determine not only the magnitude of the net magnetization in each of the successive planes in a layered material, but also the direction of that magnetic moment.

SELECTION RULES FOR SCATTERING OF POLARIZED NEUTRONS BY MAGNETIC MOMENTS

- ONLY MAGNETIZATION COMPONENTS $\perp \vec{Q}$ GIVE RISE TO SCATTERING
- COHERENT NUCLEAR SCATTERING : ALL NSF

- NUCLEAR SPIN INCOHERENT

FIELD AT SAMPLE	SF	NSF
$\vec{H} \parallel \vec{Q}$	2/3	1/3
$\vec{H} \perp \vec{Q}$	"	"

- ANTIFERROMAGNET OR PARAMAGNET

FIELD AT SAMPLE	SF	NSF
$\vec{H} \parallel \vec{Q}$	1	0
$\vec{H} \perp \vec{Q}$	1/2	1/2

- SPIRAL MAGNETIC STRUCTURES WITH SINGLE DOMAIN OF ONE CHIRALITY :

$\vec{H} \parallel \vec{Q}$ $\quad + \rightarrow -$ OR $- \rightarrow +$ SF ONLY, DEPENDING ON WHETHER SPIRAL IS RIGHT- OR LEFT-HANDED

Some other useful configurations employed in the investigation of magnetic structures in materials via scattering with polarized neutrons.

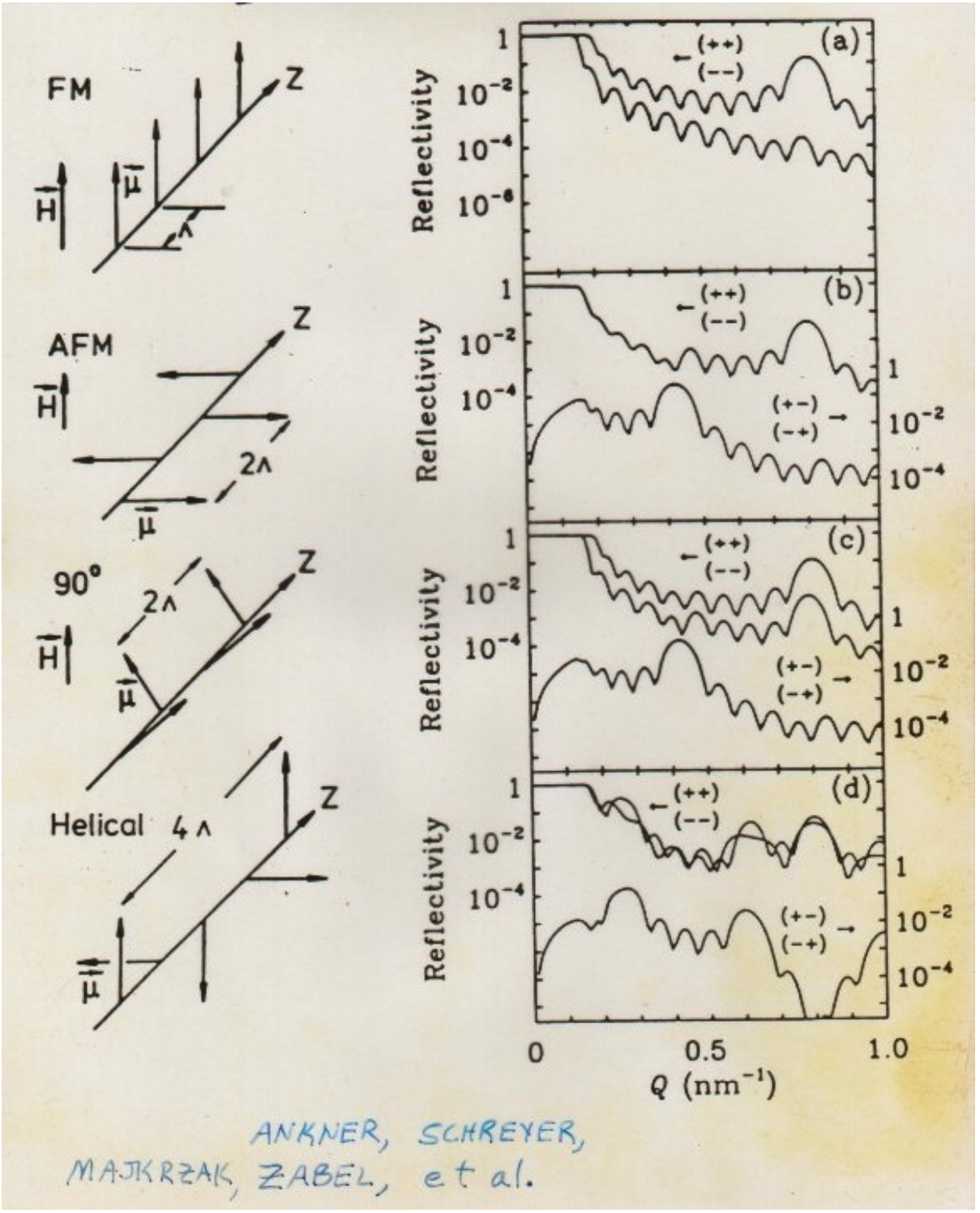

Four basic magnetic structures and their corresponding spin-dependent reflectivity curves as would be obtained with polarized neutrons.

Polarized Beam Reflectometer (PBR) at NIST

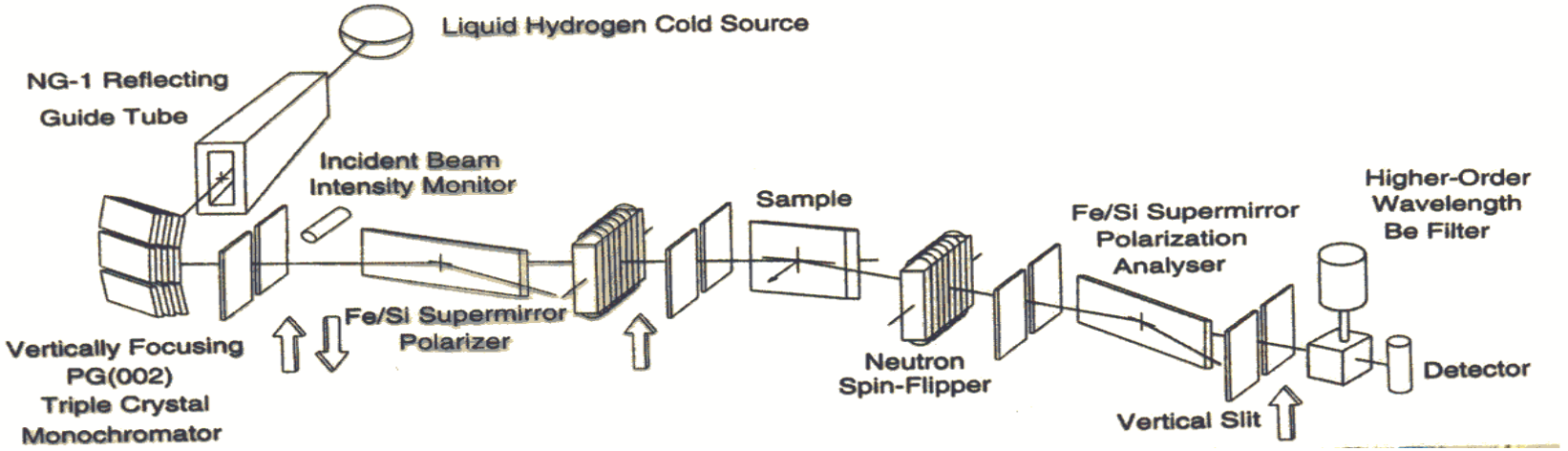

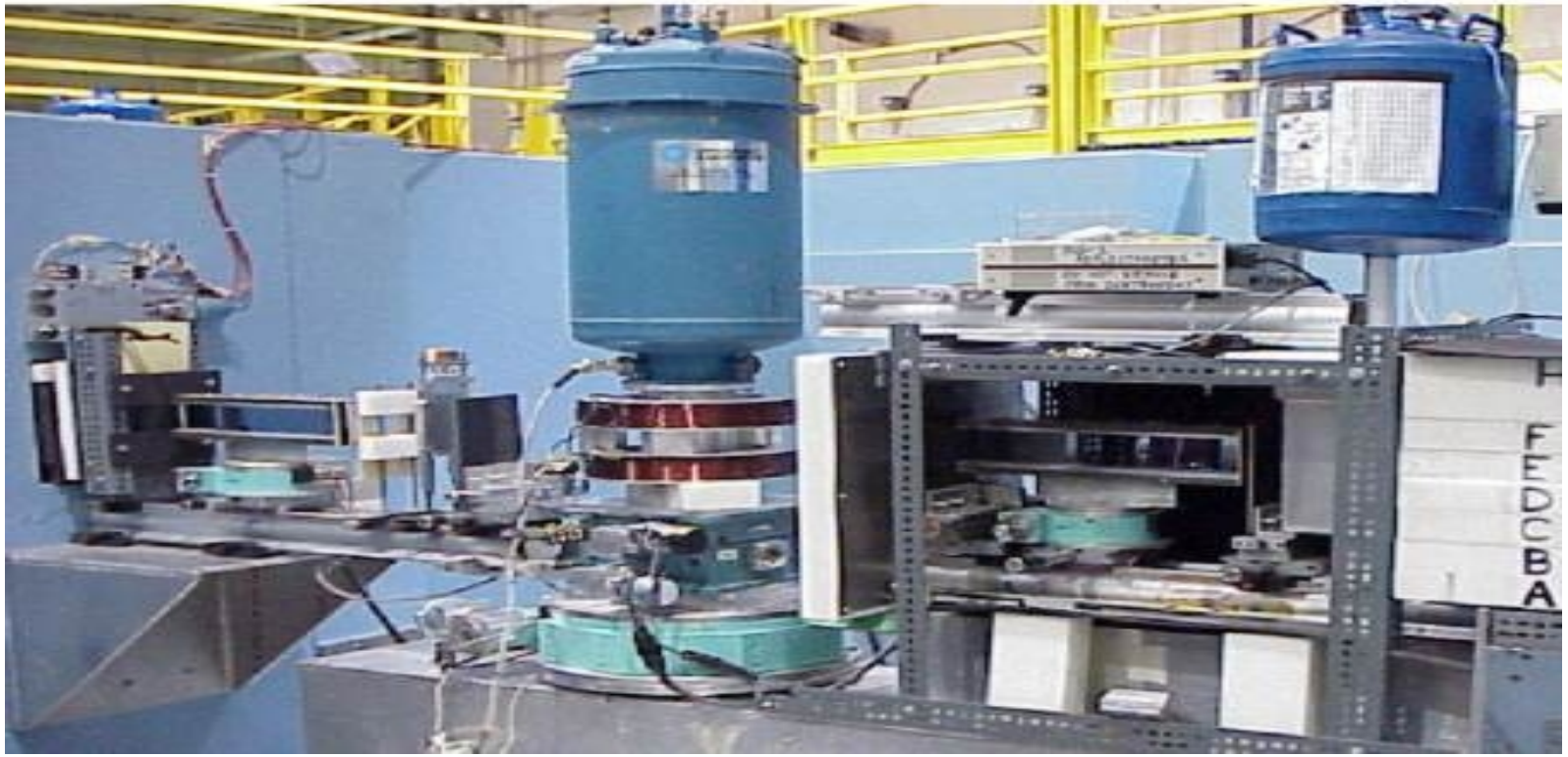

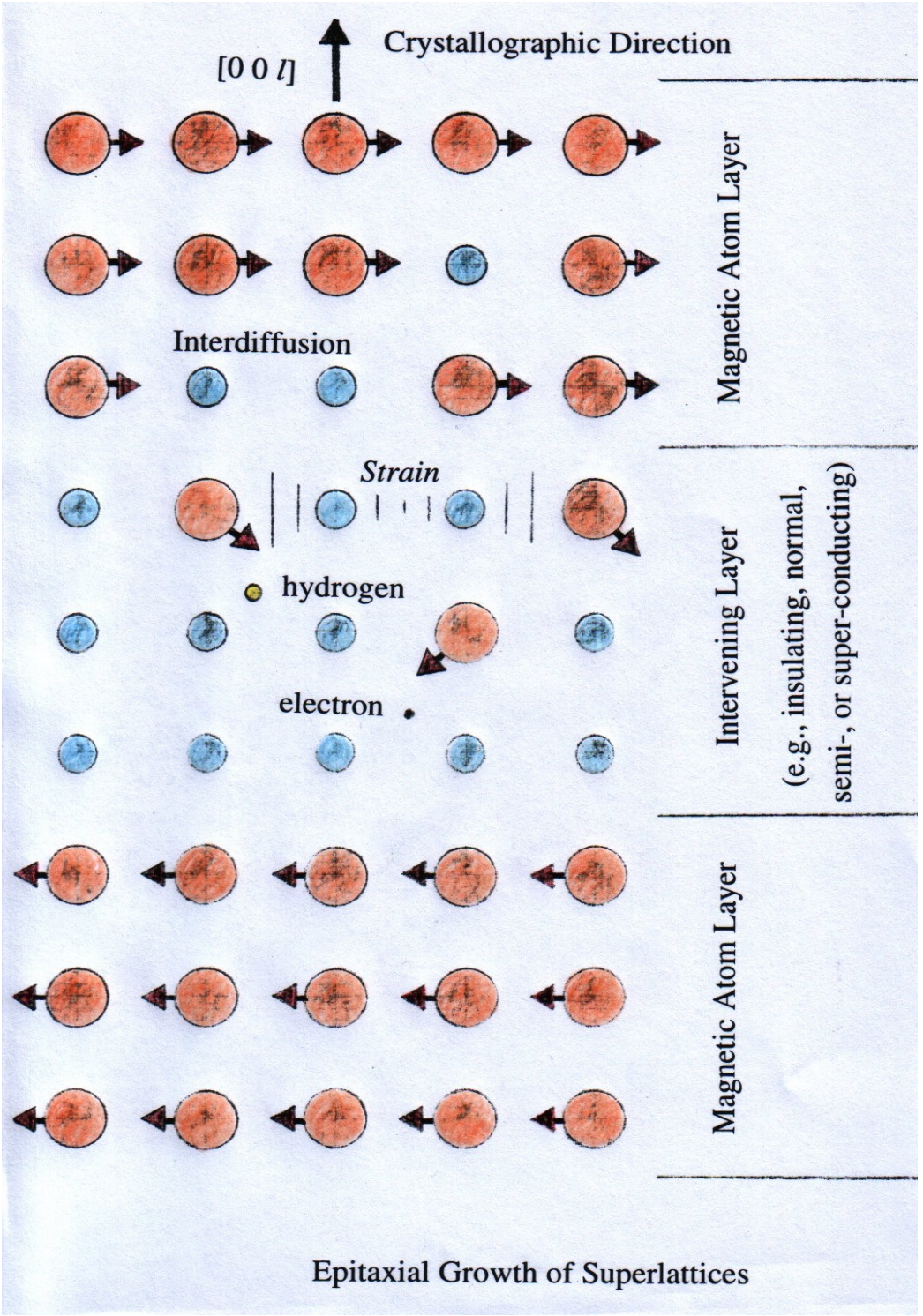

By means of molecular beam epitaxial growth in ultrahigh vacuum and other thin film deposition techniques, it is possible to construct synthetically layered systems tailored to study specific types of interactions of interest in hard condensed matter. For instance, how two separated regions made up of ferromagnetic atomic planes interact with one another across an intervening region of atomic planes of a material that is superconducting or semiconducting can be studied by analysis of the polarized neutron reflectivity -- as a function of temperature, applied magnetic field magnitude and direction, or other parameter such as the thickness of the intervening layer.

There exists a considerable body of work on systems prepared in this manner.

Magnetic Multilayers and Thin Films

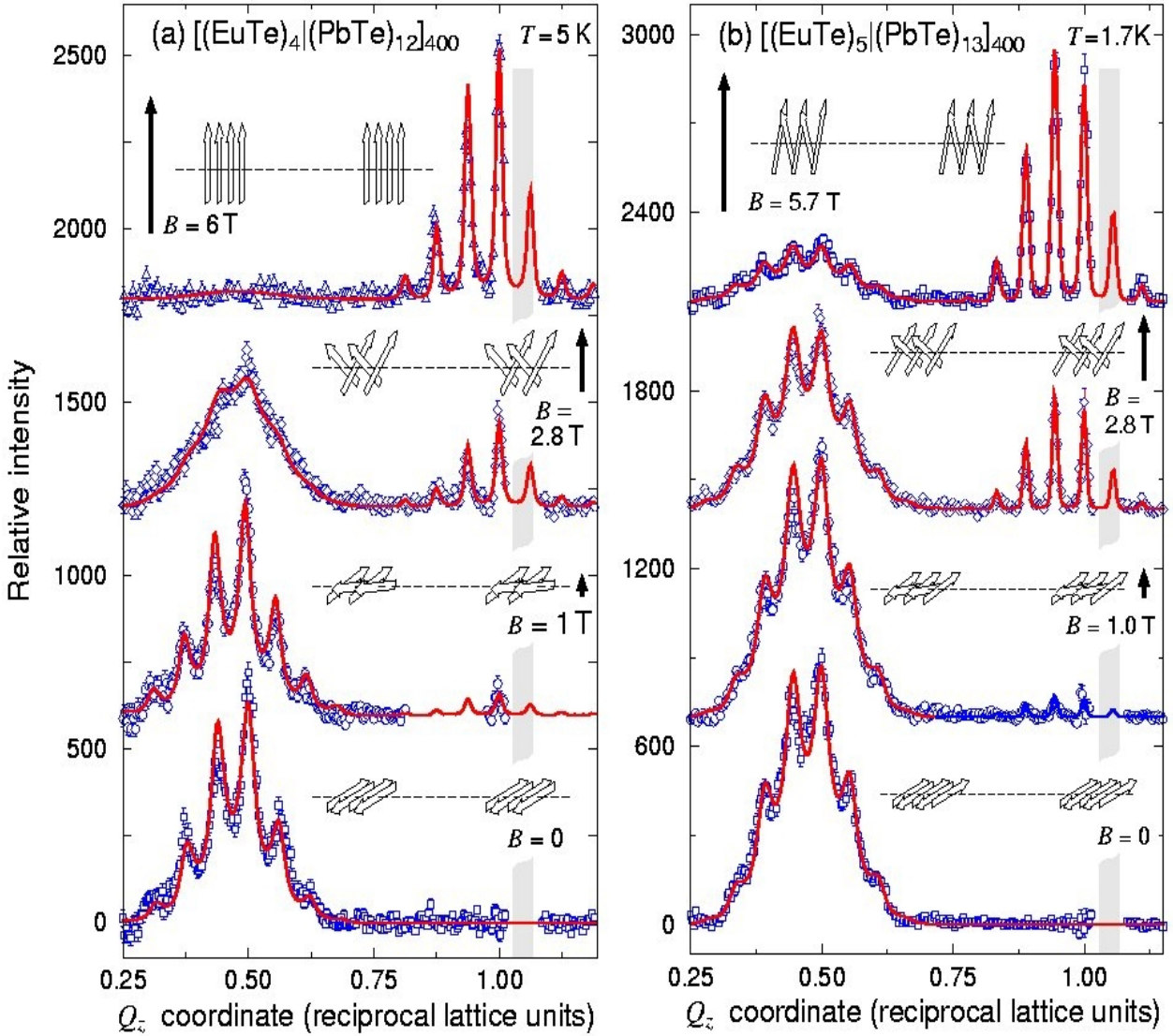

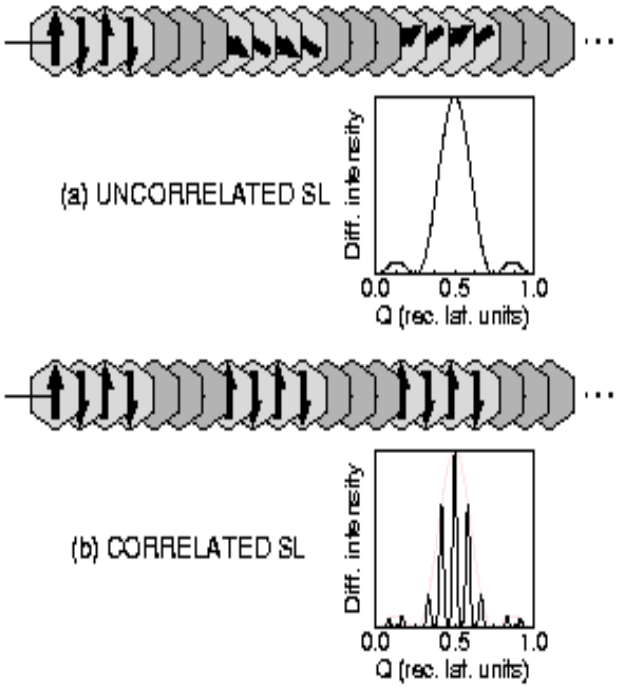

Remarkably detailed information about magnetic structure on an inter-atomic length scale can be obtained from polarized neutron reflection and diffraction studies. (Polarized neutron reflection data on magnetic semiconductor superlattices by Henryk Kepa et al..)

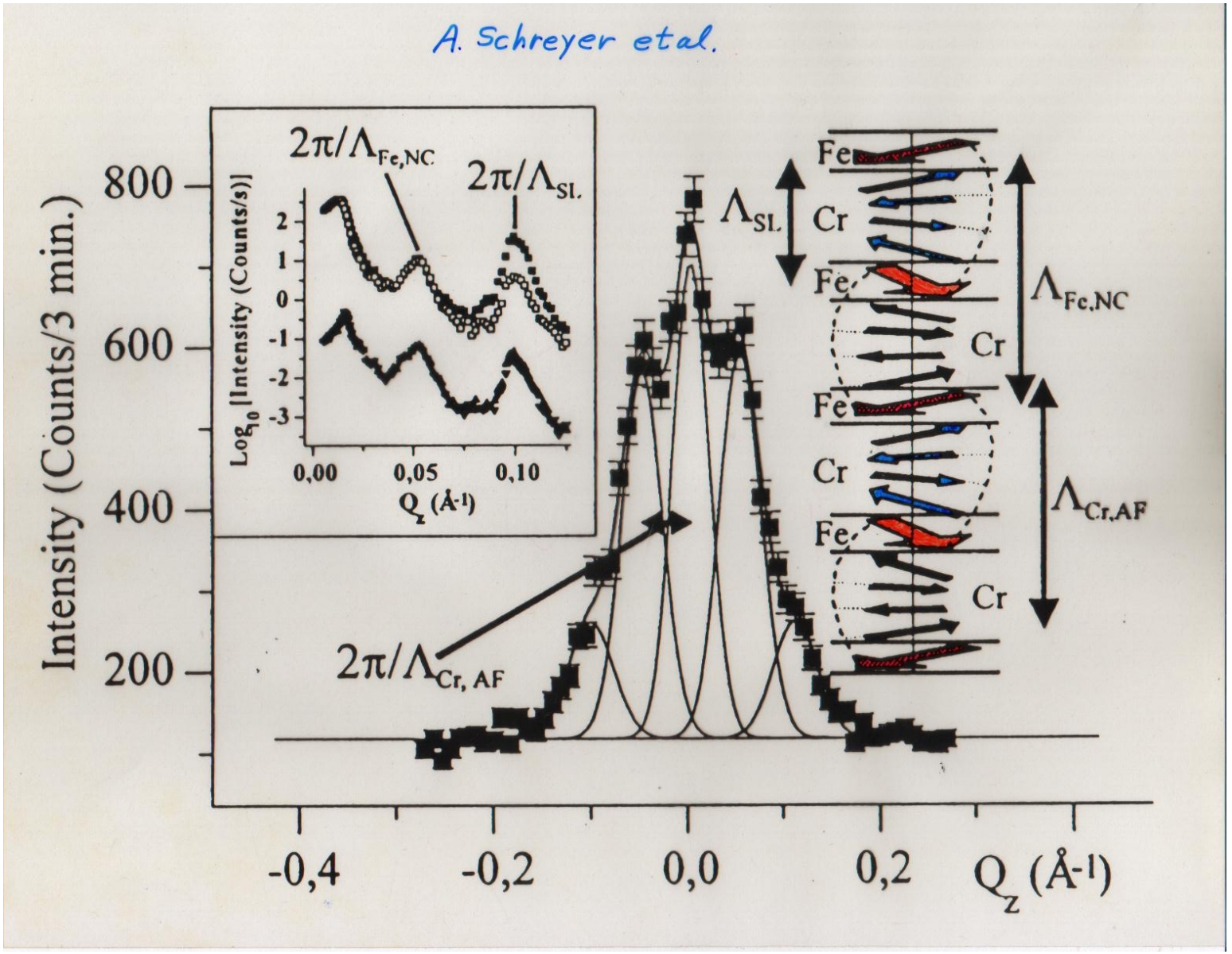

In this particular example, each ferromagnetic Fe layer consists of several atomic planes -- the relative orientations of these layers to one another within the overall layered system is deduced principally from the relatively low-Q polarized neutron reflectivity data (inset). The intricate modulated antiferromagnetic structure of the Cr atomic planes within the intervening layers is revealed primarily in the higher-Q polarized neutron diffraction pattern.

Magnetic Semiconductor Superlattices

Currently a great deal of attention is being focused on spintronics, a new area of solid-state electronics. In spintronics not only the electric current but also its spin state is controlled. Spin valves and spin injectors are the first practical applications of spintronics. Further progress in developing new devices hinges critically on the availability of suitable materials. Such materials need to be ?good? semiconductors, easy to integrate in typical integrated circuits, and their electronic properties should exhibit strong sensitivity to the carrier?s spin, ferromagnetism being an especially desirable property.

EuS is one of the very few natural ferromagnetic (F M) semiconductors. Since it becomes F M at a low temperature (T_c = 16.6 K) it is an unlikely choice for applications. However, studying the properties of heterostructures made on its base may give an important insight into fundamental processes taking place in all classes of materials under consideration.

GaMnAs is a man-made F M semiconductor. It is an example of a diluted magnetic semiconductor (D M S) in which a fraction of nonmagnetic cations (Ga) is substituted with magnetic ions (Mn). Such a material can readily be incorporated into modern GaAs-based semiconductor devices. Its T_c is still below room temperature, but this limitation may be lifted in other materials of this class (Refer to Reference 1).

Interlayer exchange coupling (I E C) in superlattices (S L), composed of ferromagnetic and nonmagnetic layers, is a crucial element of all spin-valve type devices that utilize the giant magnetoresistance effect. In metallic S L's currently being used, conduction electrons transfer the interlayer interactions through nonmagnetic spacers (Refer to Reference 2). Here we address the question whether I E C phenomena are possible in all-semiconductor superlattices, like EuS/PbS and GaMnAs/GaAs, where the carrier concentrations are many orders of magnitude lower than in metals.

The nonmagnetic spacer in EuS/PbS S L's is a narrow gap semiconductor with electron concentration of the order of 10^{17} cm^{-3} to 10^{18} cm^{-3}. For thin PbS layers (d_{PbS} < 70 Å) neutron reflectivity spectra, shown in Figure 1, have revealed a pronounced maximum of magnetic origin at the position corresponding to the doubled structural S L periodicity, thus indicating the existence of antiferromagnetic (A F M) interlayer arrangements (Refer to Reference 3).

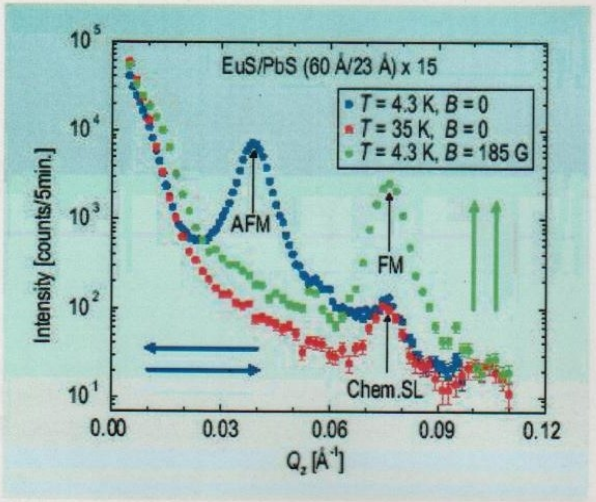

FIGURE 1. Unpolarized neutron reflectivity spectra for EuS/PbS S L with thin (23 Å) PbS spacer. Antiferromagnetic interlayer exchange coupling below T_c and at zero external field is clearly visible (blue curve). Applying a strong enough magnetic field (185 G in this case) parallel to the S L surface forces all the EuS layer?s magnetizations to ferromagnetic configuration (green curve). Above T_c the system is nonmagnetic, the only Bragg peak comes from the chemical S L periodicity.

For much thicker PbS spacers (d_{PbS} > 120 Å) the only magnetic peaks visible in the reflectivity profiles, see example in Figure 2, coincide with the chemical ones, thus leading to the conclusion that the magnetization vectors in adjacent EuS layers are parallel, which indicates F M I E C.

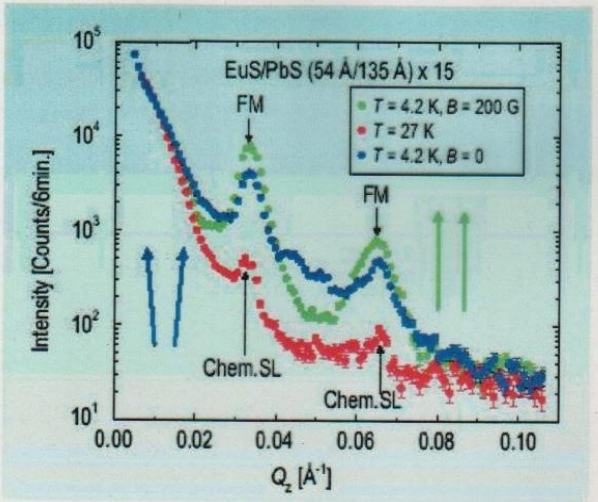

FIGURE 2. The sample with thick (135 Å) PbS layers is almost ferromagnetically coupled. Application of an external magnetic field enhances the F M Bragg peaks and lowers the intensity between them (at the A F M peak position).

In the intermediate PbS thickness range (70 Å < d_{PbS} < 120 Å), both A F M and F M peaks are present. Polarized neutron analysis of these maxima gives evidence that the magnetization vectors of adjacent EuS layers are not colinear. Hence, the I E C found in EuS/PbS S L's has an oscillatory character similar to that occurring in metallic S L's, although the oscillation period is much longer than the one in metallic systems.

In order to confirm that the free carriers, present in the PbS layer in such a small amount, are the cause of the observed oscillatory I E C, a series of analogous measurements have been carried out on EuS/YbSe S L's. The structure and lattice constant of YbSe are the same as those of PbS. In contrast to PbS, YbSe is a semi-insulator with a negligible carrier concentration. Neutron reflectivity profiles have shown no evidence of any interlayer coupling in the all investigated samples. That finding, together with the oscillatory character of coupling in S L's with PbS spacer, strongly points to the leading role of PbS free electrons in providing the necessary I E C mechanism, similar to that discovered in metallic multilayers.

Ferromagnetic ordering in GaMnAs is carrier (holes) induced; the Mn atoms, apart from being the magnetic element in the system, act also as acceptors providing the holes responsible for transferring exchange interactions between them. The details of the magnetic ordering, in particular its range, are still being disputed.

To address the latter issue, polarized neutron reflectometry has been performed on a number of GaMnAs/GaAs superlattices. Figure 3 shows an example of the obtained reflectivity profile in the vicinity of the first S L Bragg peak, for one of the samples. The very presence of the magnetic contribution to the structural S L Bragg peak is a strong confirmation of the F M I E C between consecutive GaMnAs layers. The absence of any spin-flip scattering shows that the sample is in a one-domain state, i.e., the F M ordering in GaMnAs is long range, and the sample is spontaneously saturated. The peak in (--) cross section, and its absence in the (++), is proof that the magnetization is directed oppositely to the external magnetic guide field, hence the long range ordering has formed spontaneously, without the influence of the external field. More details can be found in Reference 4.

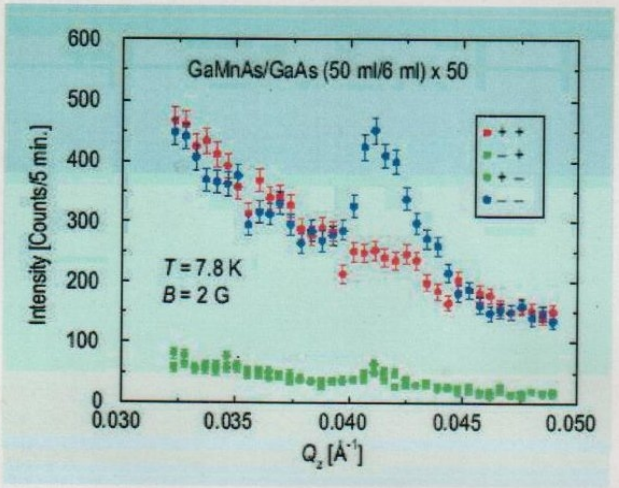

FIGURE 3. Polarized neutron reflectivity spectra for GaMnAs/GaAs superlattice.

References

[1] T. Dietl, H. Ohno, F. Matsukura, J. Cibert, D. Ferrand, Science 287,1018 (2000).

[2] P. Bruno, Phys. Rev. B52, 411 (1995).

[3] H. Kepa, J. Kutner-Pielaszek, J. Blinowski, A. Twardowski, C. F. Majkrzak, T. Story, P. Kacman, R. R. Galazka, K. Ha, H. J. M. Swagten, W. J. M de Jonge, A. Yu. Sipatov, V. Volobuev, T. M. Giebultowicz, Europhys. Lett. 56, 54 (2001).

[4] H. Kepa, J. Kutner-Pielaszek, A. Twardowski, C. F. Majkrzak, J. Sadowski, T. Story, T. M. Giebultowicz, Phys. Rev. B64, 121302 (2001).

Authors

A. Yu. Sipatov, V. Volobuev
Kharkov State Polytechnical University
Kharkov, Ukraine

H. Kepa, J. Kutner-Pielaszek, A. Twardowski
Institute of Experimental Physics
Warsaw University
Warsaw, Poland

T. Story, J. Sadowski
Institute of Physics
Polish Academy of Sciences
Warsaw, Poland

Pinpointing Chiral Structures with Front/Back Polarized Neutron Reflectometry

K. V. O'Donovan, J. A. Borchers, and C. F. Majkrzak
NIST Center for Neutron Research
National Institute of Standards and Technology
Gaithersburg, MD 20899-8562

O. Hellwig, E. E. Fullerton
IBM Almaden Research Facility
San Jose, CA 95120-6001

We have developed a new method of using polarized neutron reflectometry (PNR) to extract the structure of buried magnetic spirals in magnetic films. This technique improves upon earlier methods by being particularly sensitive to the presence of magnetic twists vis-à-vis structures in which the magnetization direction does not vary appreciably. Tracking the formation and growth of twists may solve a number of puzzles that hamper the development of magnetic thin film devices.

In collaboration with IBM scientists, we have applied the technique to a thin-film exchange-spring magnet and confirmed that the results may violate the current theory regarding the behavior of such magnets. It has been predicted that exchange-spring magnets, comprised of soft and hard ferromagnets in close proximity, are a composite that has a strong moment and does not readily demagnetize [1]. Therefore, exchange-spring magnets should give industry the ability to make much smaller permanent magnets for use in the magnetic recording devices, and elsewhere. As a side effect, when a small external magnetic field is opposed to that of the magnet, the portion of the soft ferromagnet farthest from the hard ferromagnet may twist into alignment with the field. When the field is removed, the soft ferromagnet untwists. The film provided by IBM consists of the hard ferromagnet $Fe_{55}Pt_{45}$ topped by the soft ferromagnet $Ni_{80}Fe_{20}$ [2].

Figure 1 shows a simplified diagram of the behavior predicted by current theories [1]. A magnetic field of 0.890 T, provided by an electromagnet, is sufficient to align both the soft and the hard layers of our exchange-spring magnet, as shown on the left. When a modest reverse field (on the order of 0.025 T) is applied to the exchange spring magnet, only the top of the soft layer will realign with the magnetic field. The hard layer remains pinned in the original direction, and a continuous twist is induced in the soft layer, as the direction of magnetization changes smoothly between the reverse field direction to the aligning field direction.

Although there are many alternatives to PNR to measure the magnetization, typically they measure only the average orientation of the magnetic spins, and cannot readily distinguish a spiral from a structure in which all the spins are canted with respect to an external field. PNR can extract the depth-dependence of the magnetic and chemical structure. We have studied the sample over a wide range of external magnetic fields, and can track the development of the spiral with field [3].

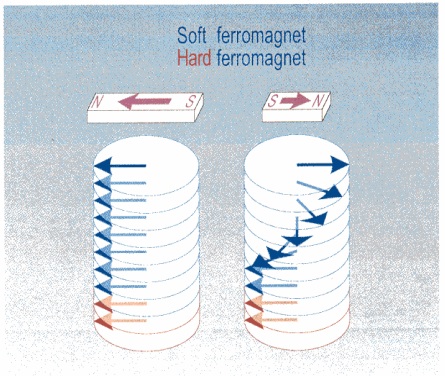

FIGURE 1. Model for field behavior of exchange-spring magnets. On the left the magnet has been aligned by a large external magnetic field. On the right a smaller field opposed to the first field causes a twist to form in the soft ferromagnet, while the hard ferromagnet remains aligned.

A PNR experiment begins with neutrons whose magnetic moments are aligned parallel (+) or opposite (–) to the external magnetic field. When the magnetization of the sample is perpendicular to this magnetic field, the neutron moment precesses as it interacts with the sample. When this happens the spin-flip (SF) reflectivities R^{+-} and R^{-+} are strong. If the magnetization of the sample is parallel to the external magnetic field, no precession occurs, but the non-spin-flip (NSF) reflectivities R^{++} and R^{--} will differ. The NSF reflectivities also provide information about the chemical structure of the film.

Our new modification of the PNR method greatly enhances the contrast between colinear and certain non-colinear magnetic structures [4]. We first measure the reflectivity with neutrons glancing off the front surface of the material, and then repeat with neutrons glancing off the back surface. The experiment is akin to holding the plane of the film up to a "magnetic mirror" to see whether the mirror image is the same as the original structure. In a colinear structure, all the spins are aligned along a common direction, and the mirror image is very much like the original structure.

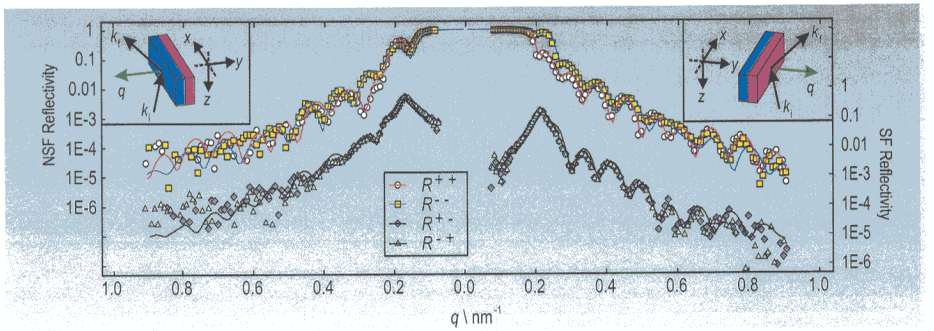

FIGURE 2. Reflectivity of a $Ni_{80}Fe_{20}|Fe_{55}Pt_{45}$ bilayer. The front reflectivity is plotted on the right while the back reflectivity is plotted on the left. The SF reflectivities R^{+-} and R^{-+} are plotted against the right ordinate axis. The NSF reflectivities R^{++} and R^{--} are plotted against the left ordinate axis.

But the mirror image of a magnetic twist to the right is a magnetic twist to the left. Therefore, if the front and back reflectivities are significantly different, we can deduce the presence of a spiral. Fitting the data confirms the spiral's existence.

Figure 2 shows data collected at 0.026 T after aligning in -0.89 T. Fits to the data are shown as solid lines. The data from the front reflectivity are shown on the right, and the data from the back reflectivity are shown on the left. The spin-flip (SF) reflectivities R^{+-} and R^{-+} are plotted against the right-hand axis, which have been shifted relative to the NSF reflectivities R^{++} and R^{--} plotted against the left axis. At $q = 0.2$ nm^{-1}, there is a splitting in the front NSF reflectivity that is much more pronounced than that of the back reflectivity at the same q. This is a hallmark of the spiral structure.

Figure 3 shows the magnetic structure that gives the excellent fit to the data plotted in Fig. 2. The location of the hard/soft interface is marked in Fig. 3. Surprisingly, we discover the spiral invades the hard ferromagnet even at extremely low fields. Current theory predicts that when this occurs, the soft ferromagnet will not be able to untwist fully. Yet, other magnetic studies show that our exchange-spring magnet does untwist when this field is removed. Thus, our PNR measurements have identified a shortcoming of current theory.

With this new technique, NIST is now able to better characterize the magnetic properties of thin films, which can improve the capability and reliability of industrial devices for magnetic recording and sensing.

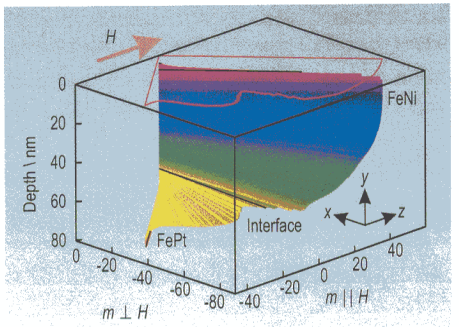

FIGURE 3. Fitted magnetization of the data presented in Fig. 2. The front of the sample is at a depth of 0 nm and the back is at a depth of 70 nm. The red curve is a projection of the magnetic structure into the plane of the front surface.

References

[1] E. F. Kneller and R. Hawig, IEEE Trans. Magn. **27**, 3588 (1991).

[2] O. Hellwig, J. B. Kortright, K. Takano, and E. E. Fullerton, Phys. Rev. **B62**, 11694 (2000).

[3] K. V. O'Donovan, *et al.*, in preparation.

[4] K. V. O'Donovan, *et al.*, submitted to Applied Physics A.

The Nobel Prize in Physics 2007

This year's Nobel Prize in Physics is awarded to ***ALBERT FERT*** *and* ***PETER GRÜNBERG*** *for their discovery of Giant Magnetoresistance. Applications of this phenomenon have revolutionized techniques for retrieving data from hard disks. The discovery also plays a major role in various magnetic sensors as well as for the development of a new generation of electronics. The use of Giant Magnetoresistance can be regarded as one of the first major applications of nanotechnology.*

Better read-out heads for pocket-size devices

Constantly diminishing electronics have become a matter of course in today's IT-world. The yearly addition to the market of ever more powerful and lighter computers is something we have all started to take for granted. In particular, hard disks have shrunk – the bulky box under your desk will soon be history when the same amount of data can just as easily be stored in a slender laptop. And with a music player in the pocket of each and everyone, few still stop to think about how many cds' worth of music its tiny hard disk can actually hold. Recently, the maximum storage capacity of hard disks for home use has soared to a terabyte (a thousand billion bytes).

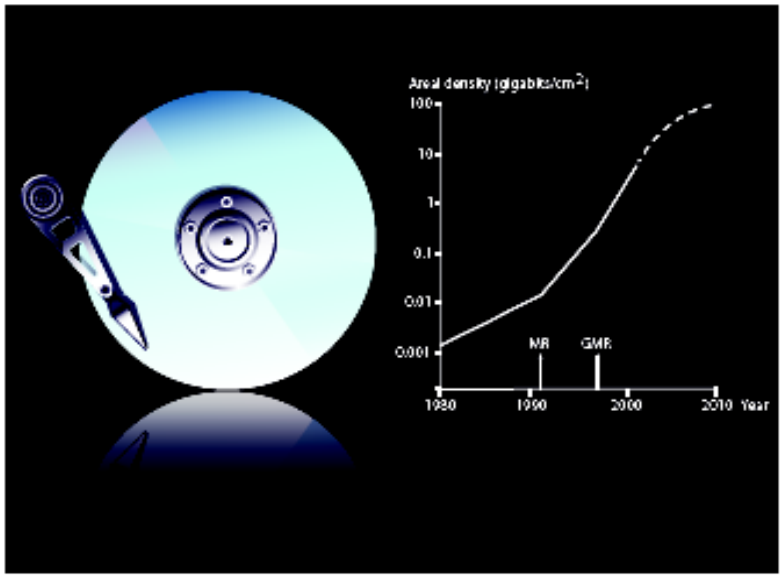

Diagrams showing the accelerating pace of miniaturization might give a false impression of simplicity – as if this development followed a law of nature. In actual fact, the ongoing IT-revolution depends on an intricate interplay between fundamental scientific progress and technical fine tuning. This is just what the Nobel Prize in Physics for the year 2007 is about.

9 October 2007

KUNGL. VETENSKAPSAKADEMIEN
THE ROYAL SWEDISH ACADEMY OF SCIENCES

Scientific Background on the Nobel Prize in Physics 2007

The Discovery of Giant Magnetoresistance

compiled by the Class for Physics of the Royal Swedish Academy of Sciences

The Royal Swedish Academy of Sciences, Information Department, Box 50005, SE-104 05 Stockholm, Sweden
Phone: +46 8 673 95 00, Fax: +46 8 15 56 70, E-mail: info@kva.se, Website: www.kva.se

As recounted in the “Scientific Background” material referred to on the left side of the page, prior to the discovery of the GMR effect by Gruenberg, polarized neutron diffraction studies of magnetic superlattices revealed an unambiguous coupling between magnetic layers across intervening nonmagnetic spacers. The interlayer coupling (IEC) observed in this neutron diffraction work was explained in terms of long-range exchange interactions, for example, the RKKY (Ruderman Kittel Kasuya Yosida) interaction. Interestingly, the underlying mechanism responsible for GMR was thus known about before the effect itself was discovered!

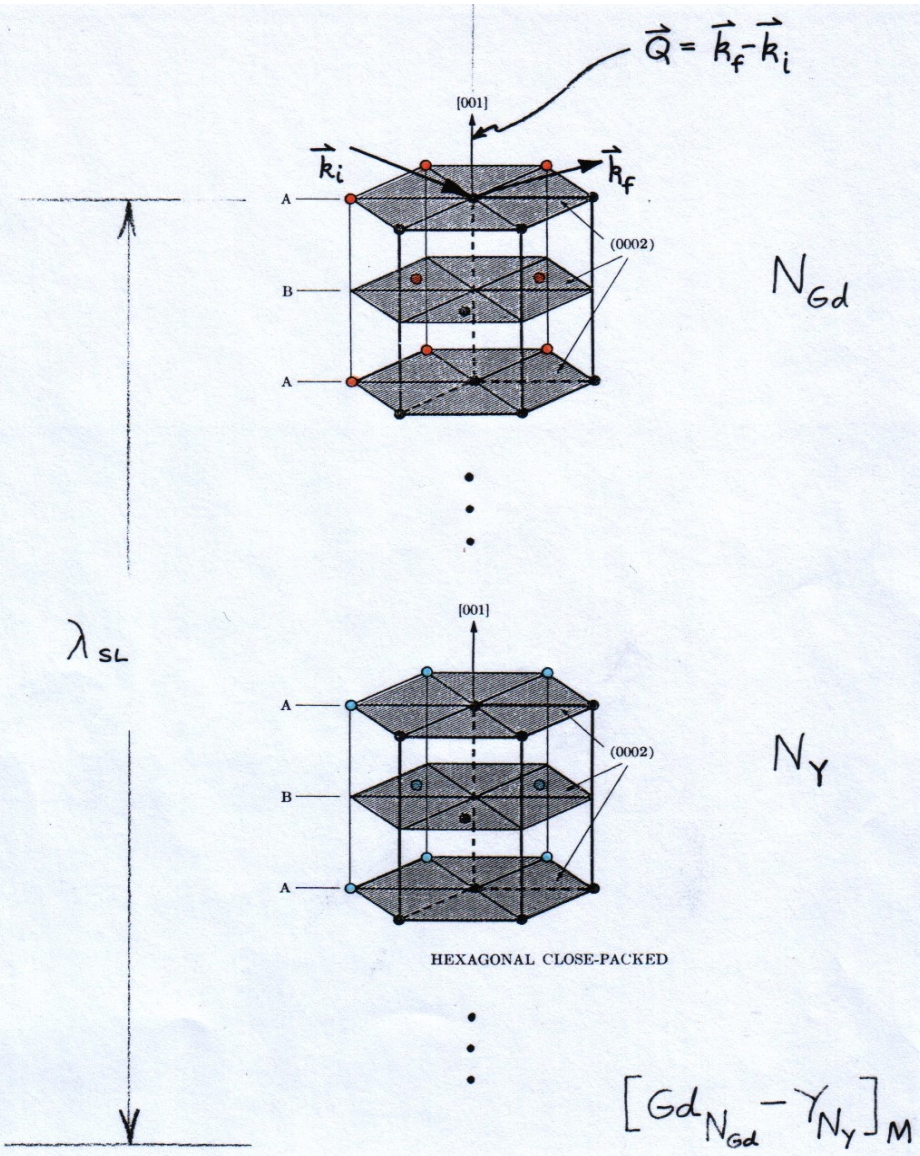
$\vec{Q} = \vec{k}_f - \vec{k}_i$
[001]
$\vec{k}_i$
$\vec{k}_f$
A
B
A
(0002)
N_{Gd}
λ_{SL}
[001]
A
B
A
(0002)
N_Y
HEXAGONAL CLOSE-PACKED
$[Gd_{N_{Gd}} - Y_{N_Y}]_M$
Y(002) SEED LAYER
Nb (110) BUFFER LAYER
Al_2O_3 $(11\bar{2}0)$ SUBSTRATE

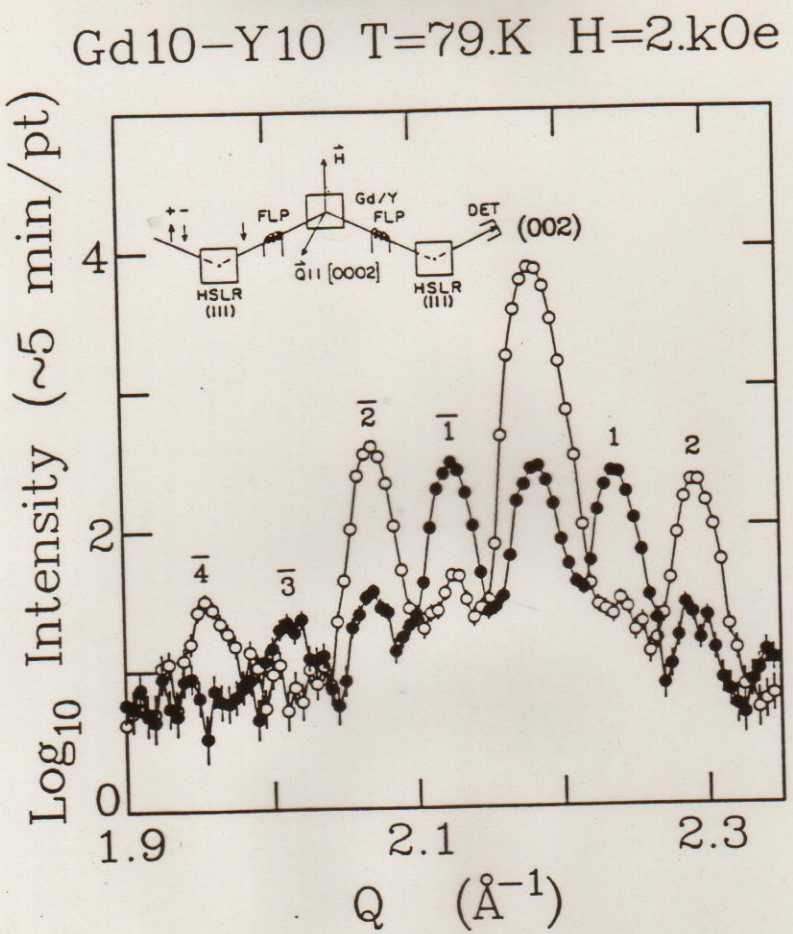

Fig. 7–1

Figure 7-1. NSF (open circles) and SF (filled circles) scattering from a [Gd_{10} - Y_{10}] superlattice as described in the text. The data have not been corrected for instrumental polarizing and flipping efficiencies (the SF scattering at the (002) position is predominantly, if not entirely, instrumental in origin). The SF scattering which appears at values of Q corresponding to a doubling of the chemical bilayer spacing (odd-numbered satellites) is consistent with an antiferromagnetic alignment (for an applied field approaching zero) of neighboring ferromagnetic Gd layers as depicted schematically in Figure 7-2. (After Majkrzak et al. (1986)).

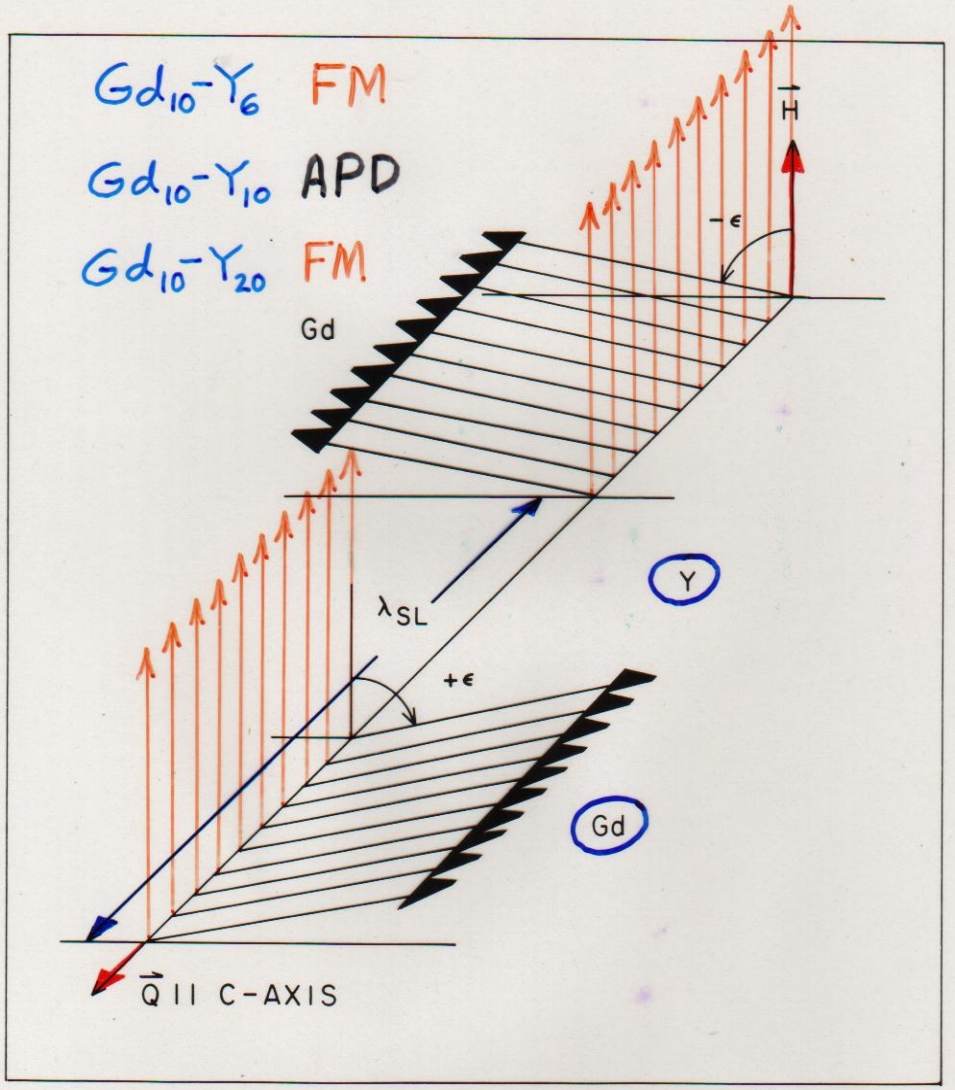
Gd_{10}-Y_6 FM
Gd_{10}-Y_{10} APD
Gd_{10}-Y_{20} FM
Gd
H
$-\epsilon$
λ_{SL}
$+\epsilon$
Y
Gd
$\vec{Q}$ II C-AXIS

• n-diffr. meas.

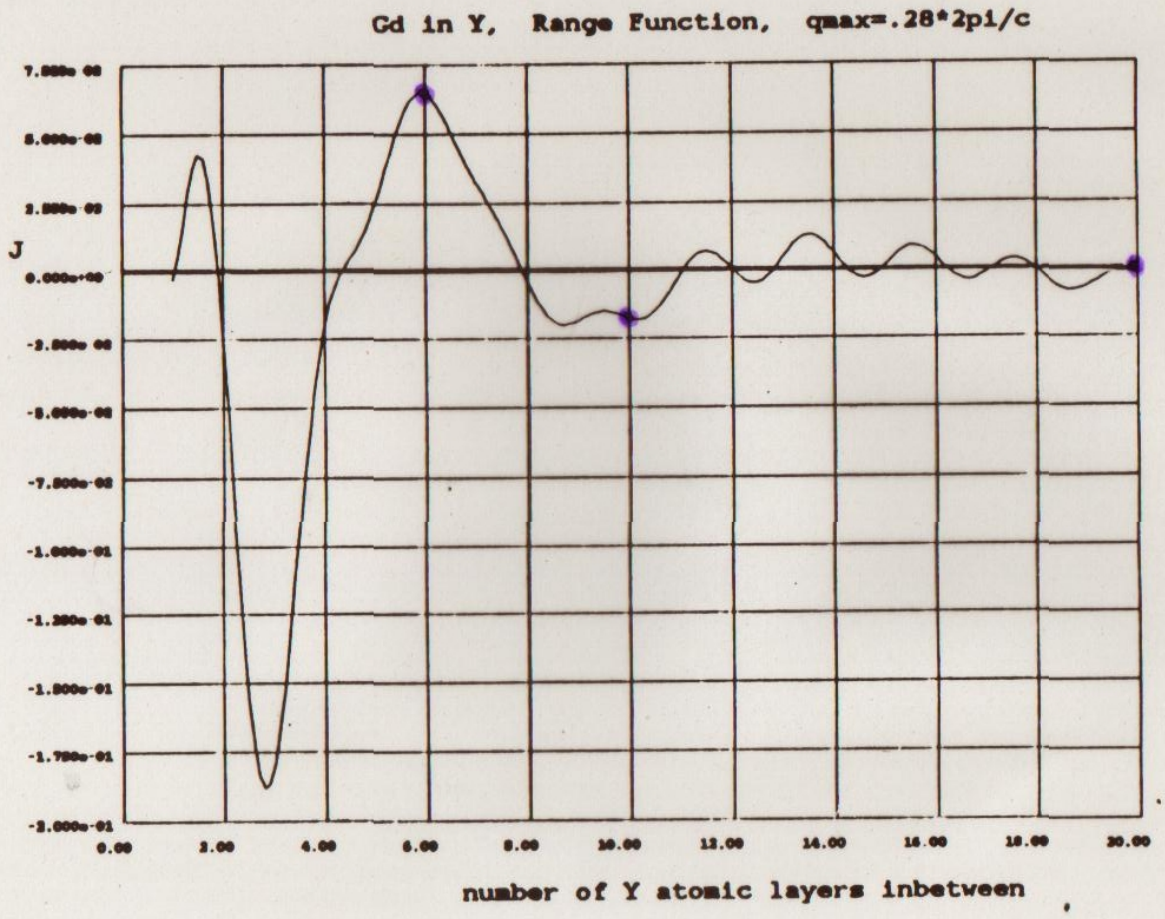
Gd in Y, Range Function, qmax=.28*2pi/c
J
0.00
2.00
4.00
6.00
8.00
10.00
12.00
14.00
16.00
18.00
20.00
number of Y atomic layers inbetween

TRANSVERSE AFM

FM SDW

Fe Cr

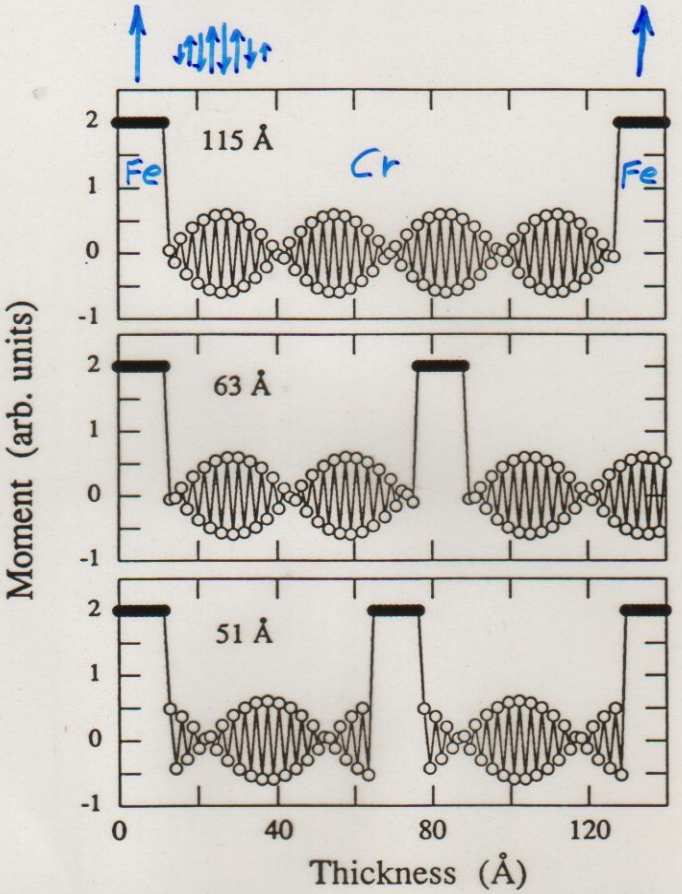

Fe/Cr SUPERLATTICES (GMR)

FULLERTON, BADER, & ROBERTSON

Figure 3

SCHREYER, ZEIDLER, ZABEL, ANKNER, MAJKRZAK, SCHÄFER, & GRÜNBERG, THIS CONFERENCE

NON COLLINEAR Fe/Cr (001)

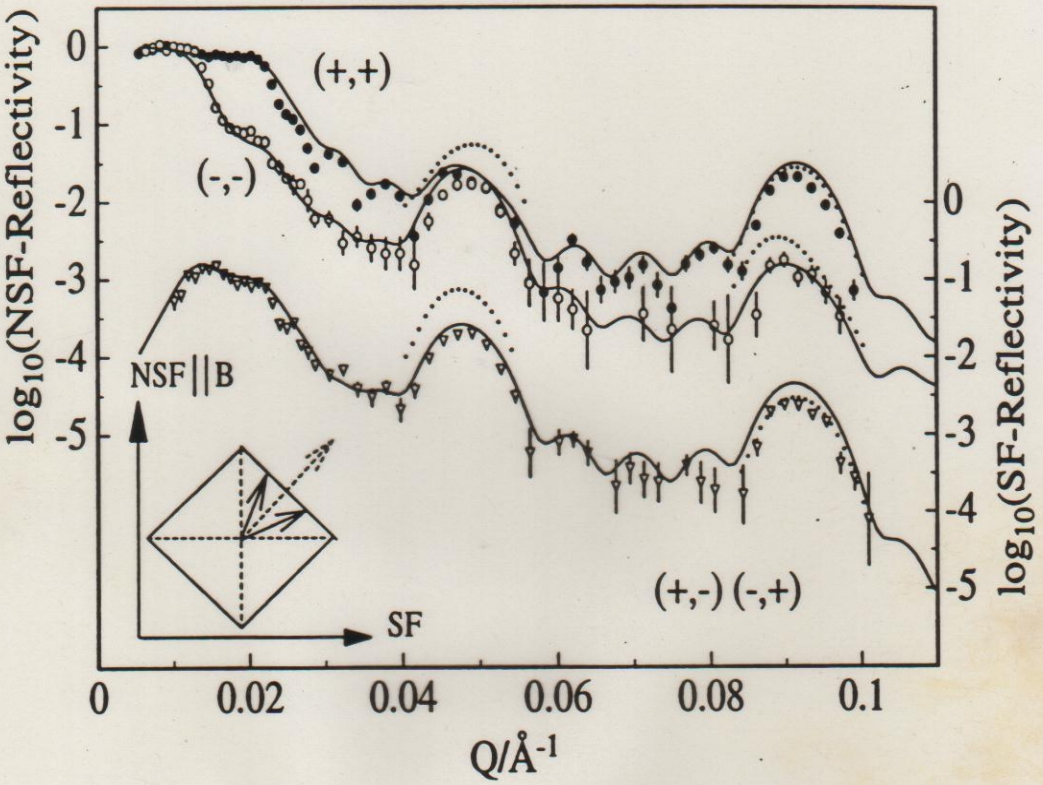

..... 90° ∡

— 50° ∡

$$E = -J_1 \frac{\vec{M}_1 \cdot \vec{M}_2}{|\vec{M}_1||\vec{M}_2|} - J_2 \left(\frac{\vec{M}_1 \cdot \vec{M}_2}{|\vec{M}_1||\vec{M}_2|} \right)^2$$

EXCHANGE COUPLING

BILINEAR

BIQUADRATIC

Part 3: Application of polarized neutrons and ferromagnetic reference layers to phase-sensitive neutron reflectometry studies of the structure of soft condensed matter systems

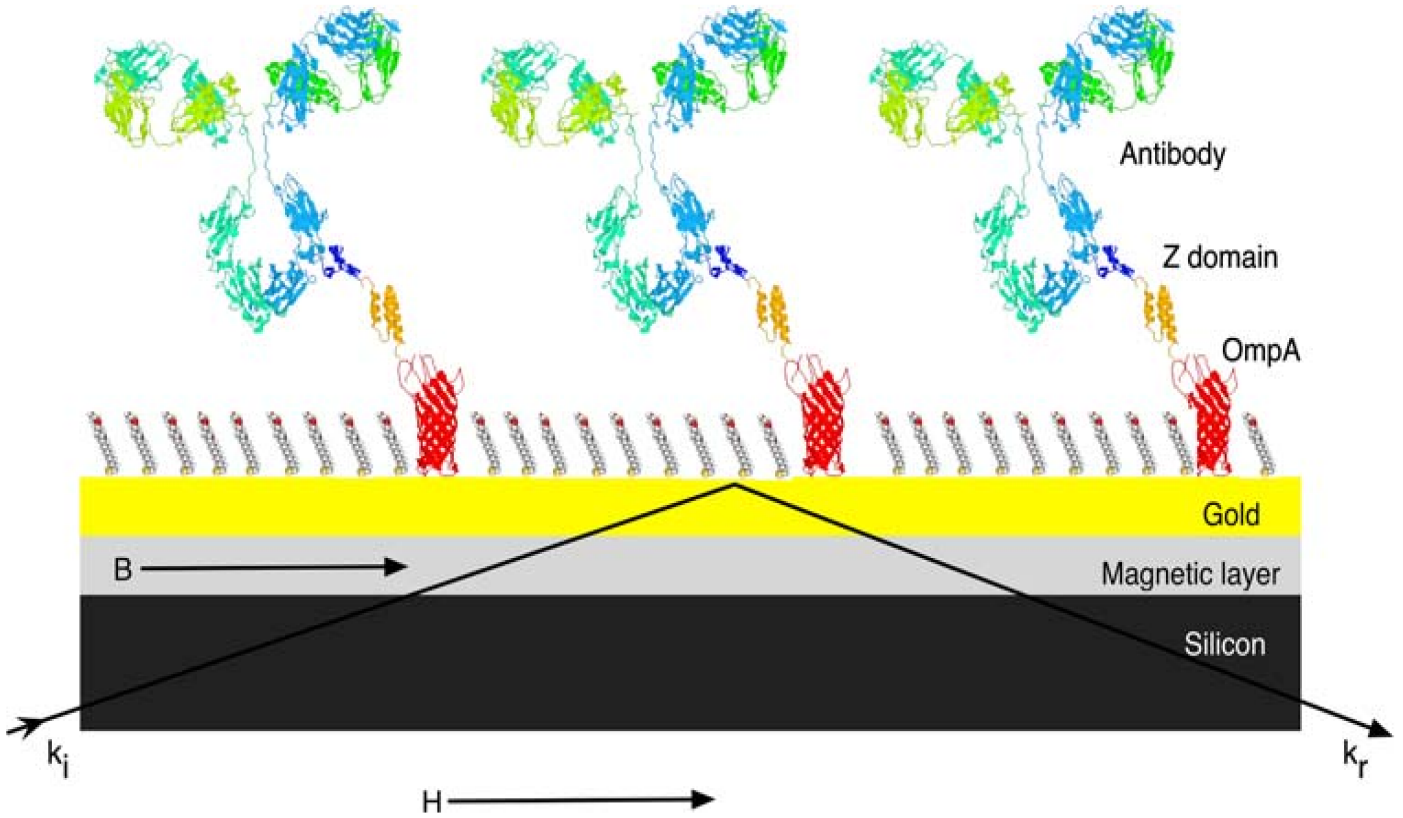

(Figure from the work of Anton Le Brun et al.)

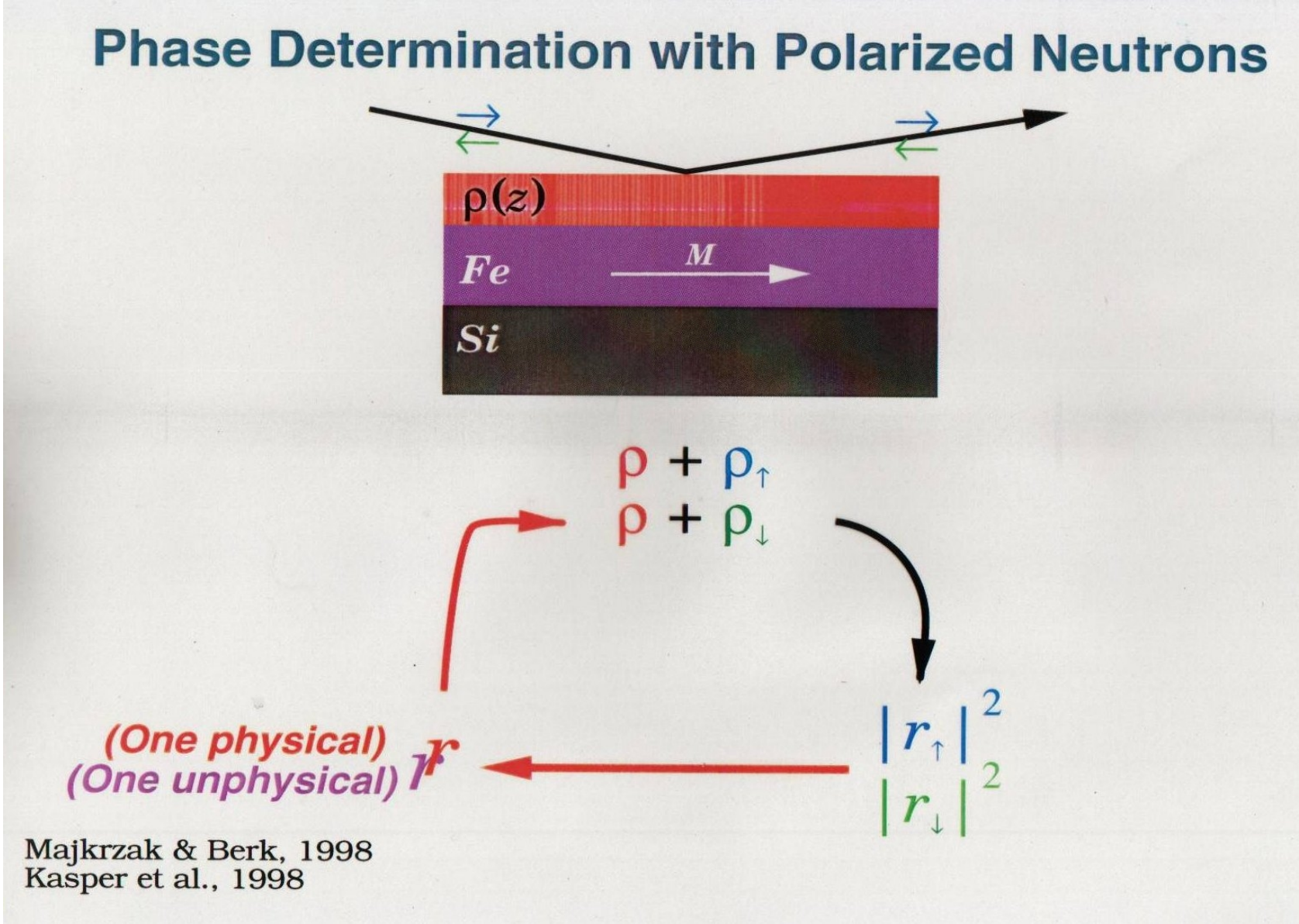

One significant advantage of using a saturated ferromagnetic material and polarized neutron beams as a means of performing phase-sensitive reflectometry is that the magnetic layer, which serves as the reference, can be chemically isolated from the non-magnetic material film whose SLD profile is of primary interest.

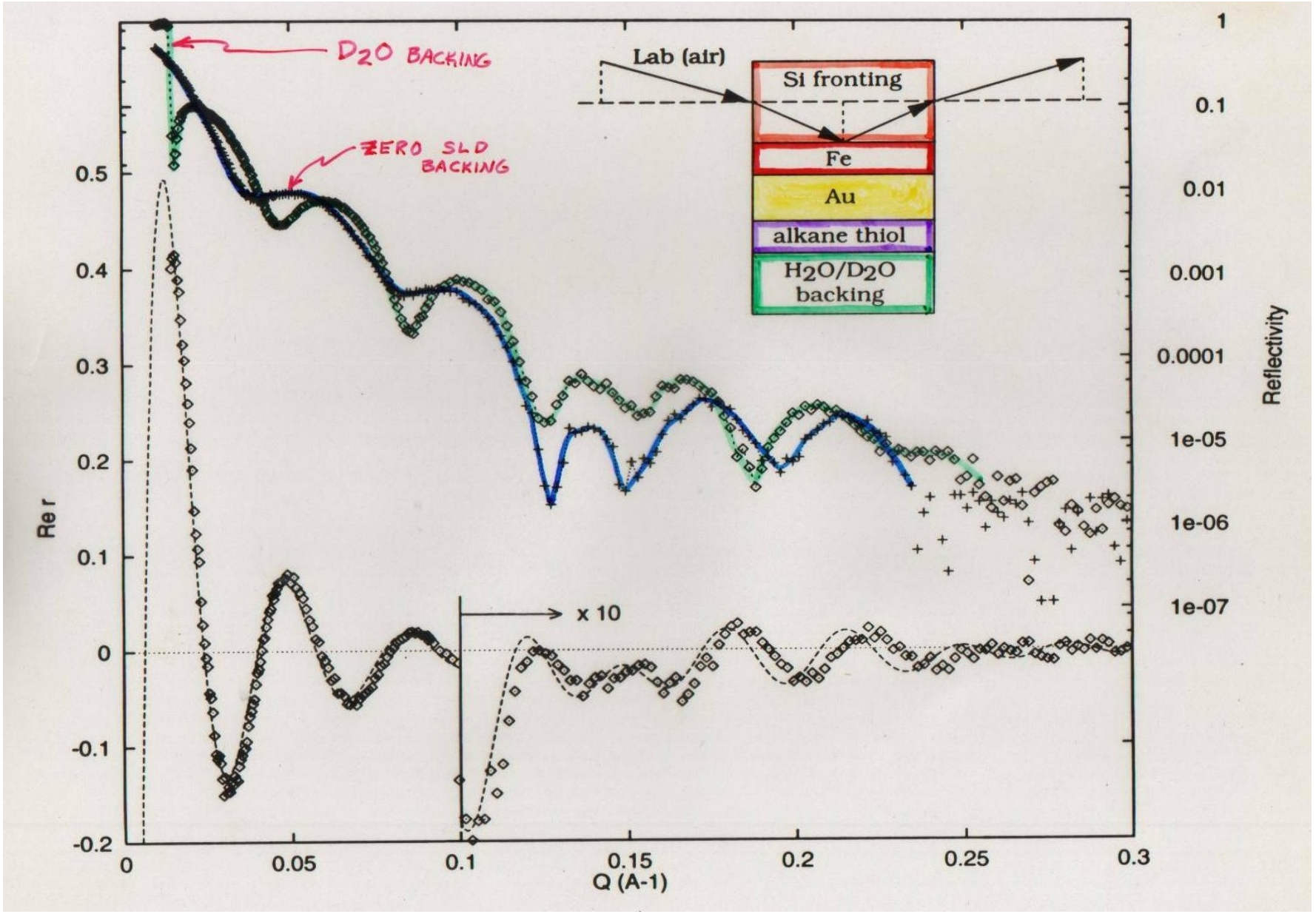

Variation of the surround (aqueous reservoir backing medium) can be used to first determine the SLD depth profile of the ferromagnetic Fe layer to be used, subsequently, as a reference layer itself.

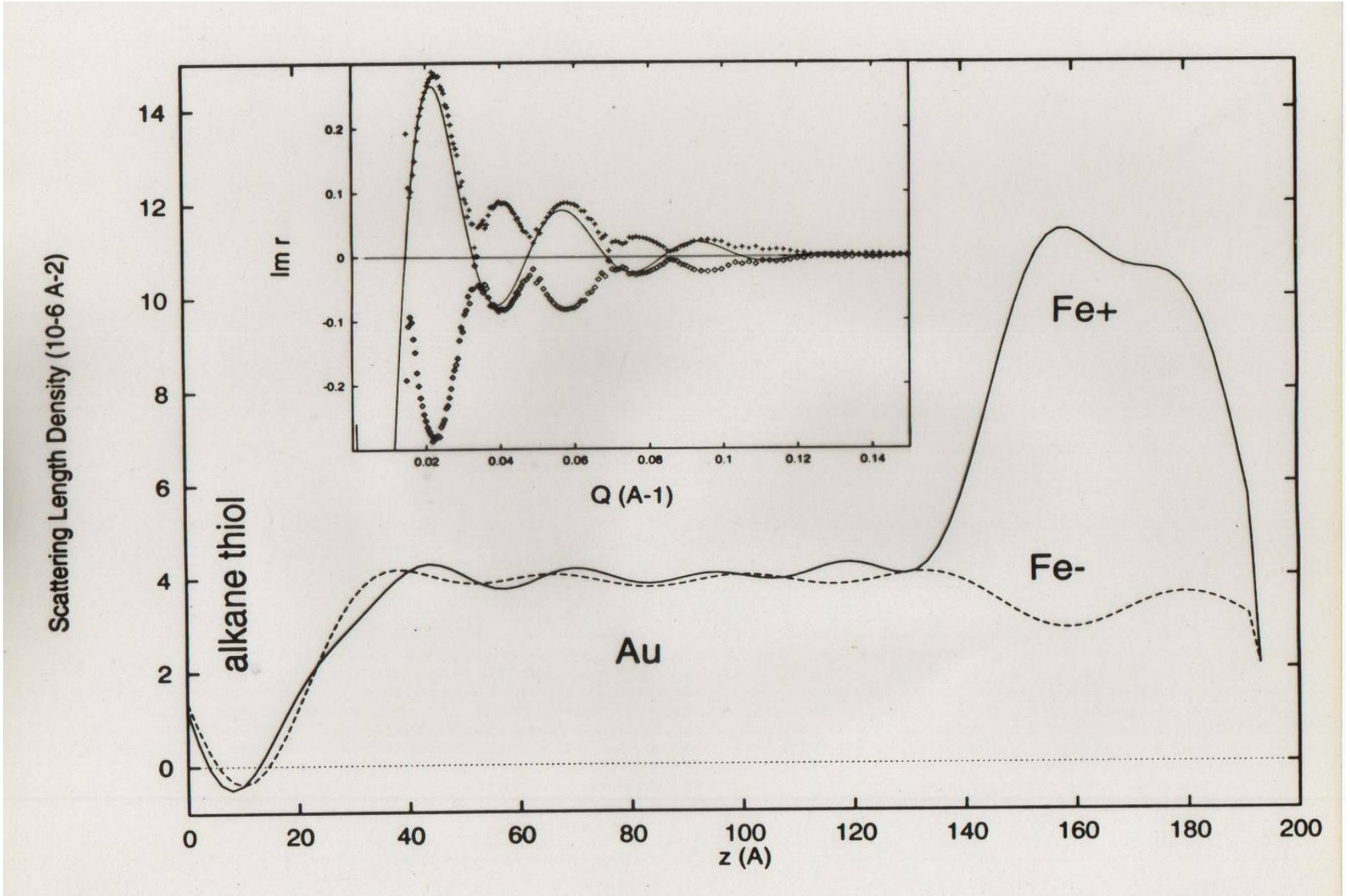

Analysis of the reflectivity data on the preceding slide yields the SLD profile plotted above -- note that the entire SLD depth profile of the composite film structure is obtained, including that of the Fe layer.

Substrate/β-ME Characterization

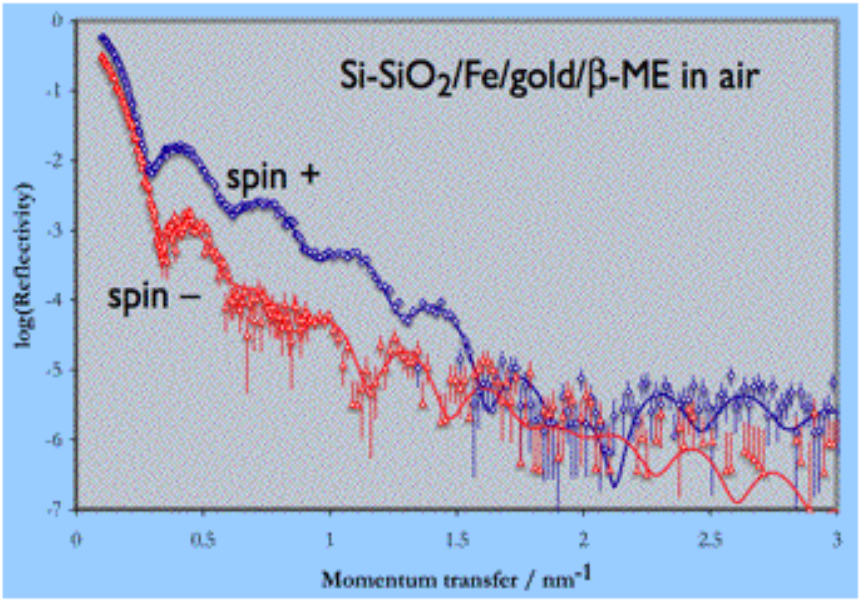

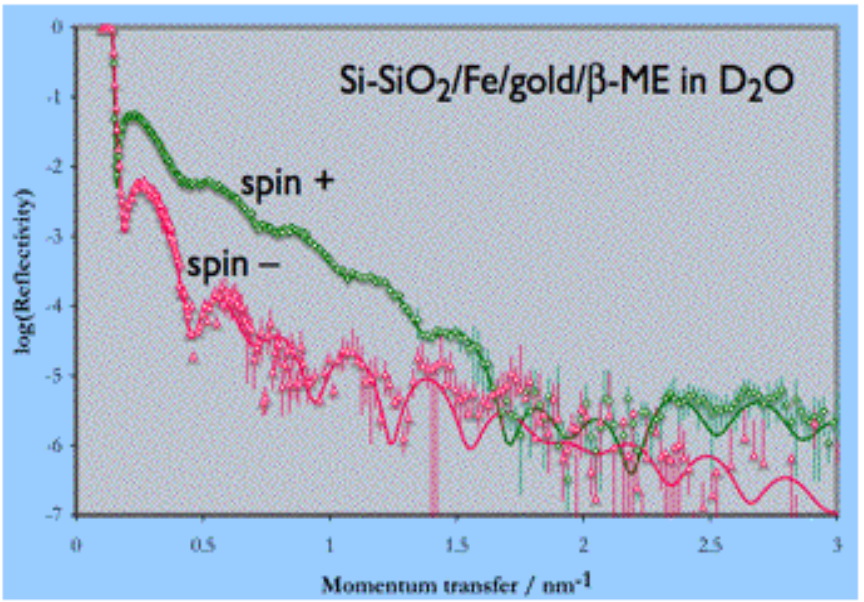

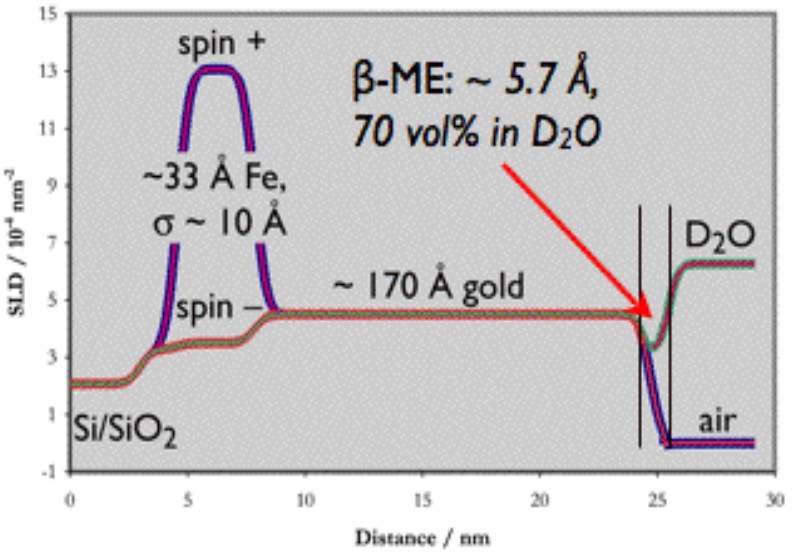

- unique neutron capability
- visualize structures that are otherwise "invisible"

McGillivray & Holt, unpublished data

An ion-channel-containing model membrane: structural determination by magnetic contrast neutron reflectometry†

Stephen A. Holt,*[a] Anton P. Le Brun,[b] Charles F. Majkrzak,[c] Duncan J. McGillivray,‡[c] Frank Heinrich,[cd] Mathias Lösche[cd] and Jeremy H. Lakey[b]

Received 15th December 2008, Accepted 17th March 2009
First published as an Advance Article on the web 20th May 2009
DOI: 10.1039/b822411k

To many biophysical characterisation techniques, biological membranes appear as two-dimensional structures with details of their third dimension hidden within a 5 nm profile. Probing this structure requires methods able to discriminate multiple layers a few Ångströms thick. Given sufficient resolution, neutron methods can provide the required discrimination between different biochemical components, especially when selective deuteration is employed. We have used state-of-the-art neutron reflection methods, with resolution enhancement *via* magnetic contrast variation to study an oriented model membrane system. The model is based on the *Escherichia coli* outer membrane protein OmpF fixed to a gold surface *via* an engineered cysteine residue. Below the gold is buried a magnetic metal layer which, in a magnetic field, displays different scattering strengths to spin-up and spin-down neutrons. This provides two independent datasets from a single biological sample. Simultaneous fitting of the two datasets significantly refines the resulting model. A β-mercaptoethanol (βME) passivating surface, applied to the gold to prevent protein denaturation, is resolved for the first time as an 8.2 ± 0.6 Å thick layer, demonstrating the improved resolution and confirming that this layer remains after OmpF assembly. The thiolipid monolayer (35.3 ± 0.5 Å), assembled around the OmpF is determined and finally a fluid DMPC layer is added (total lipid thickness 58.7 ± 0.9 Å). The dimensions of trimeric OmpF in isolation (53.6 ± 2.5 Å), after assembly of lipid monolayer (57.5 ± 0.9 Å) and lipid bilayer (58.7 ± 0.9 Å), are precisely determined and show little variation.

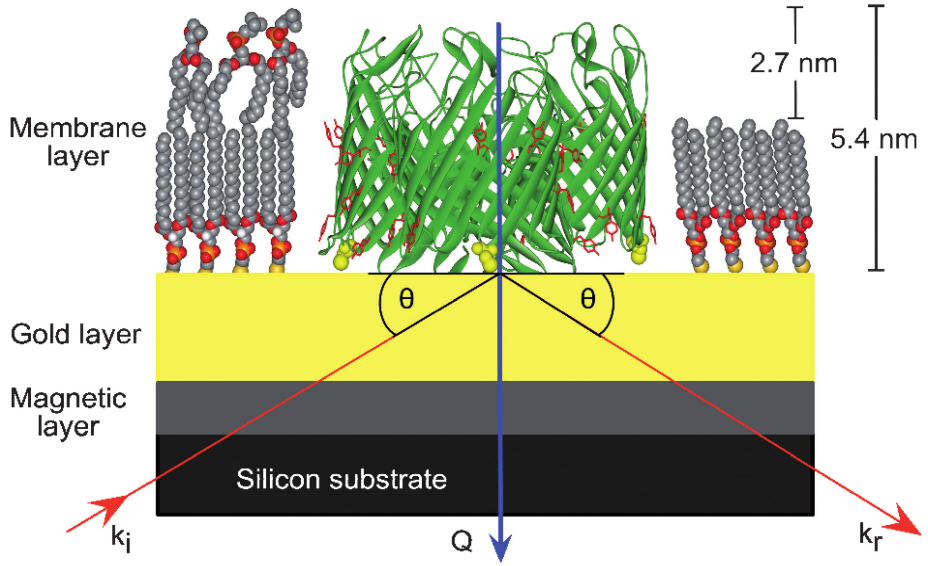

Fig. 1 Schematic of the sample configuration for the neutron reflection studies. The substrate was exposed to a 1% (v/v) βME in ethanol solution.[32] OmpF-E183C (300 μg ml^{-1} in buffer A) was incubated on the gold surface for at least 3 hours at room temperature. After incubation, the surface was washed, first with a 2% (w/v) SDS solution and then with distilled water, to remove any non-specifically bound protein. Thiolipid DPPTE (1,2-dipalmitoyl-*sn*-glyero-3-phosphothioethanol), (1.0 mg ml^{-1} in buffer A), was then deposited to infill around the OmpF trimers (right-hand side of figure). Finally DMPC (10 mg ml^{-1} in ethanol) was added to the assembled surface (left-hand side of figure) and incubated for 5 minutes. The DMPC solution was removed by washing the cell quickly with 50 ml of buffer B. The figure shows an OmpF trimer (PBD 2OMPF[34]) attached to the gold *via* cysteine residues surrounded by DPPTE (pdb file 870160.mol from Avanti Polar Lipids). DMPC molecules used to represent the upper layer are taken from a simulated DMPC bilayer structure.[61] The cysteine residues are yellow and space-filled, and a belt of tyrosine residues (wire frame, red) delineates the bilayer interface in the bacterial membrane region. The incident neutron beam (red arrow labelled k_i) was directed to reflect (k_r) from the back of the complex interfacial structure. The blue arrow labelled Q shows the scattering vector.

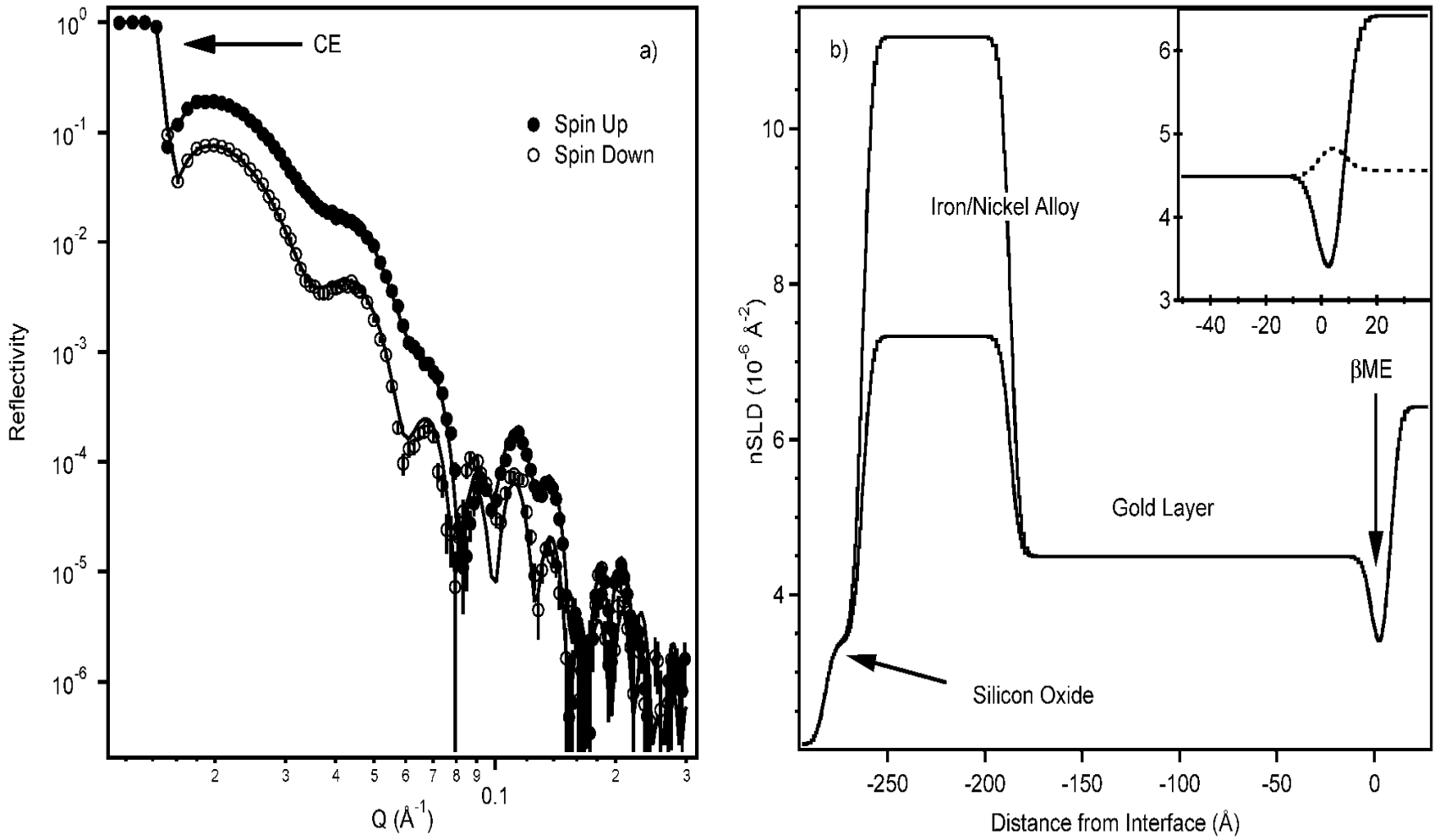

Fig. 2 a) Reflectivity data (symbols) and fit (lines) after βME adsorption onto the surface, D_2O buffer. Below the critical edge (CE) the neutrons are totally externally reflected and the reflectivity is unity. Q is the scattering vector defined in eqn (1). The separation in the data results from the different contrast of the magnetic layer to spin-up and spin-down neutrons. b) Real-space nSLD profile corresponding to the fit shown in a). The zero point has been set at the interface between the gold and the βME. The silicon substrate is on the left and D_2O buffer on the right. The twp different nSLD values for the magnetic layer are clearly seen. The hydrogenous βME layer is clearly evident between the gold and the buffer. The inset shows the βME region of the sample expanded with the dashed line the fit obtained with d-βME next to a gold-matched water buffer. Note: Data presented in Figs. 2 and 4 are all from successive depositions on the same substrate.

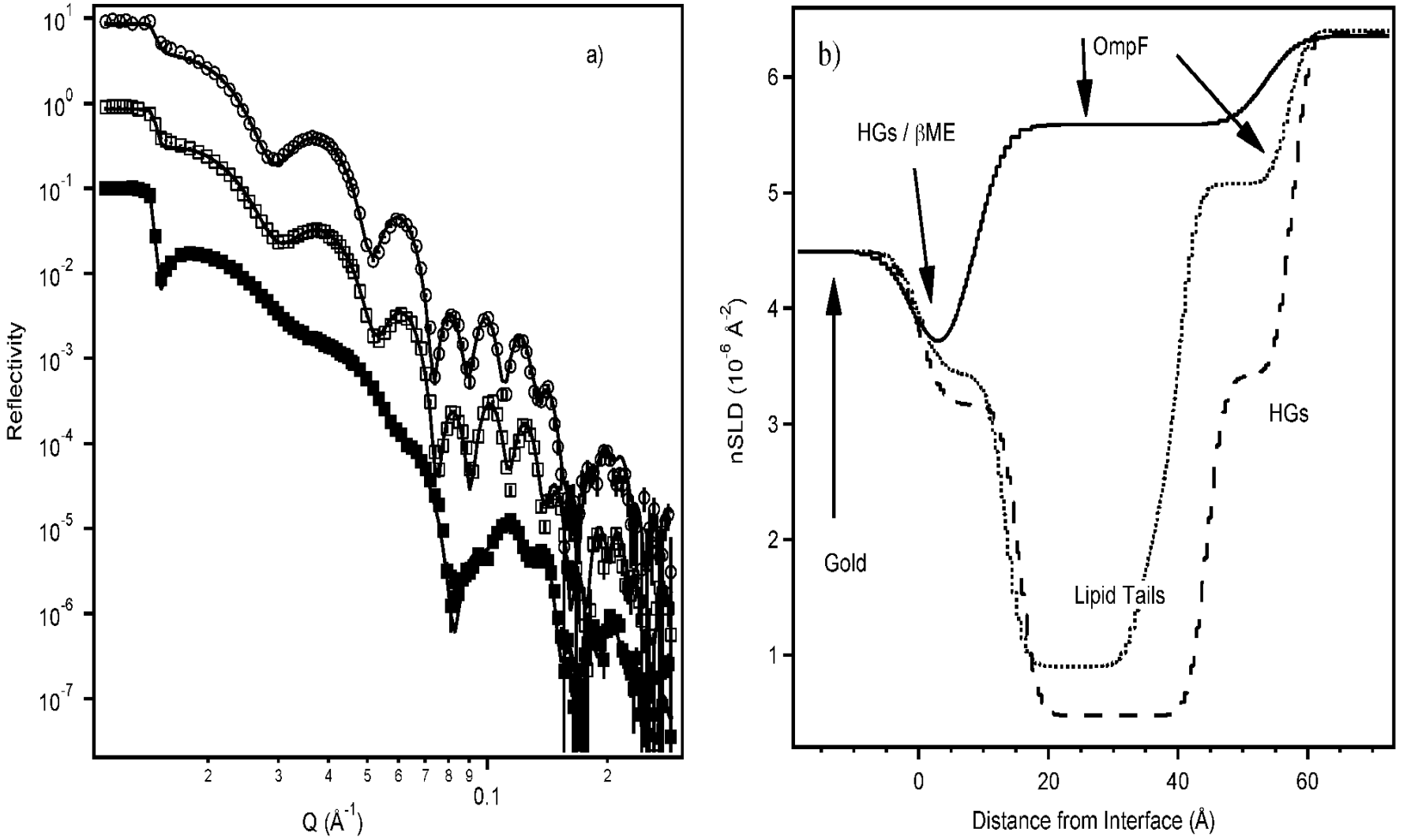

Fig. 4 a) Data, 'up polarisation' state (symbols) and fit (lines) after OmpF adsorption to a βME-passivated gold surface (■), subsequent DPPTE adsorption (□) and subsequent precipitation of DMPC (○). The OmpF and DMPC datasets have been offset for clarity. b) The real-space nSLD profiles corresponding to the fits of all polarisation data. Solid line – OmpF adsorption; dots – DPPTE adsorption; dashes – DMPC adsorption. The figure has been labelled to illustrate the main constituent of each region; HGs indicate regions of lipid headgroup.

Biomaterials 32 (2011) 3303–3311

Contents lists available at ScienceDirect

Biomaterials

journal homepage: www.elsevier.com/locate/biomaterials

The structural orientation of antibody layers bound to engineered biosensor surfaces

Anton P. Le Brun [a,1], Stephen A. Holt [b,1], Deepan S.H. Shah [c], Charles F. Majkrzak [d], Jeremy H. Lakey [a,*]

[a] Institute for Cell and Molecular Biosciences, The Medical School, Newcastle University, Framlington Place, Newcastle upon Tyne NE2 4HH, United Kingdom
[b] ISIS Neutron Facility, STFC Rutherford Appleton Laboratory, Harwell Science and Innovation Campus, Didcot, Oxfordshire OX11 0QX, United Kingdom
[c] Orla Protein Technologies Ltd, Biosciences Centre, International Centre for Life, Times Square, Newcastle upon Tyne NE1 4EP, United Kingdom
[d] NIST Centre for Neutron Research, National Institute for Standards and Technology, Gaithersburg, MD 20899, USA

ARTICLE INFO

Article history:
Received 23 December 2010
Accepted 8 January 2011
Available online 7 February 2011

Keywords:
Magnetism
Protein
Surface analysis
Surface modification
Gold
Immunochemistry

ABSTRACT

This paper describes a membrane protein array that binds immunoglobulin G at its constant regions whilst leaving the variable regions free to bind antigen. The scaffold of the array is the transmembrane domain of outer membrane protein A (tOmpA) from *Escherichia coli* engineered to assemble as an oriented monolayer on gold surfaces *via* a single cysteine residue. Other protein domains can be fused to the N and C termini of the scaffold. In this study we use circularly permuted ctOmpA fused to two Z domains of *Staphylococcus aureus* protein A (ZZctOmpA) to create the immunoglobulin G-binding array. The solution structure of the engineered proteins was assessed by circular dichroism spectroscopy. Assembly of the array, attachment of antibodies and antigen binding were measured using surface plasmon resonance and neutron reflection. Compared to mouse IgG2, polyclonal IgG from rabbit bound very strongly to ZZctOmpA and the dissociation of the immunoglobulin was slow enough to allow neutron reflection studies of the assembled layer with antigen. Using both magnetic and isotopic contrasts a complete layer by layer model was defined which revealed that the 223 Å high layer contains antibodies in an upright orientation.

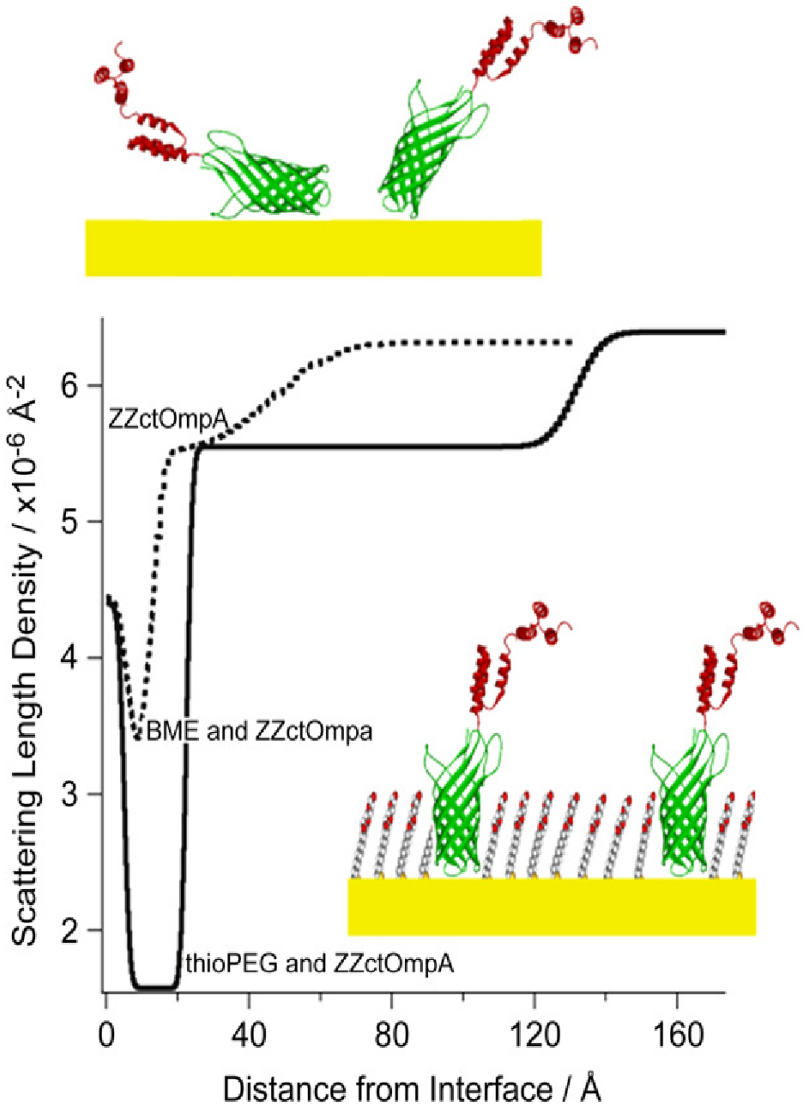

Fig. 3. The SLD profiles of ZZctOmpA immobilised to gold surface before (dotted line) and after (solid line) thioPEG deposition. The figure shows that when there is only protein and BME present on the surface the protein only layer is ill-defined. Once the filling molecule, thioPEG is added the protein is able to adopt a uniform orientation and the expected thickness of ZZctOmpA is observed.

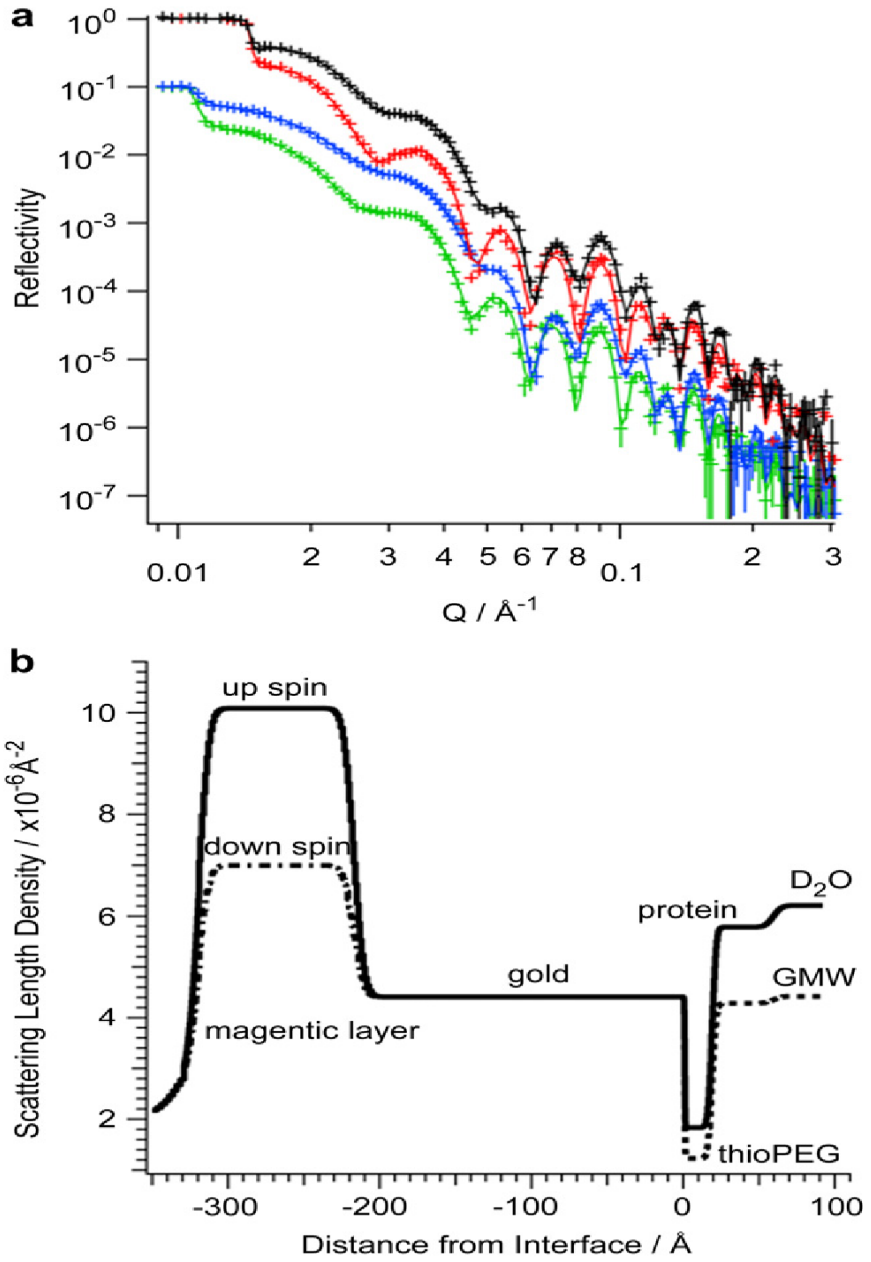

Fig. 4. a) The reflectivity of an array of ctOmpA in a D_2O (black spin up and red spin down) and gold matched water (GMW) where the SLD is matched to gold (blue spin up and green spin down). The crosses with error bars are the collected data and the solid lines the fits. The GMW data is offset for clarity. b) The corresponding SLD profile of the ctOmpA array with the gold—membrane interface set at 0 Å. The SLD of the μ-metal from spin down neutrons and the membrane layer in GMW are shown as dashed lines.

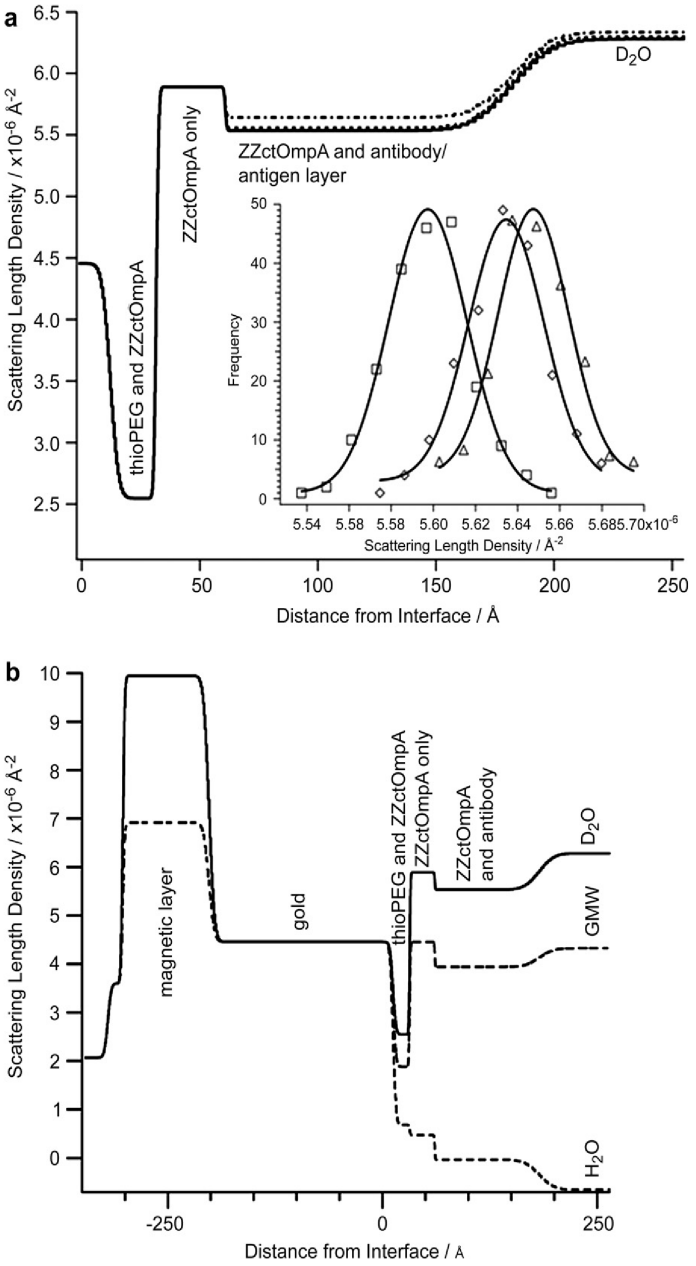

Fig. 7. a) The SLD profile of a ZZctOmpA array (from the reflectivity profiles in Supplementary Fig. S6) with the addition of rabbit polyclonal anti-HSA IgG (solid line), followed by the addition of antigen, HSA (dotted line). The final addition to the array is a secondary antibody, anti-rabbit IgG produced in goat (dashed line). All profiles are of the D_2O only subphase. The inset show the output from the MC analysis for the SLD of the ZZctOmpA antibody layer with rabbit anti-HSA IgG only (squares), after the addition of HSA (diamonds) and the final addition of anti-rabbit IgG produced in goat (triangles). The Gaussians are drawn as a guide. b) The SLD profile of rabbit anti-HSA IgG bound to an array of ZZctOmpA under magnetic and solvent contrasts.

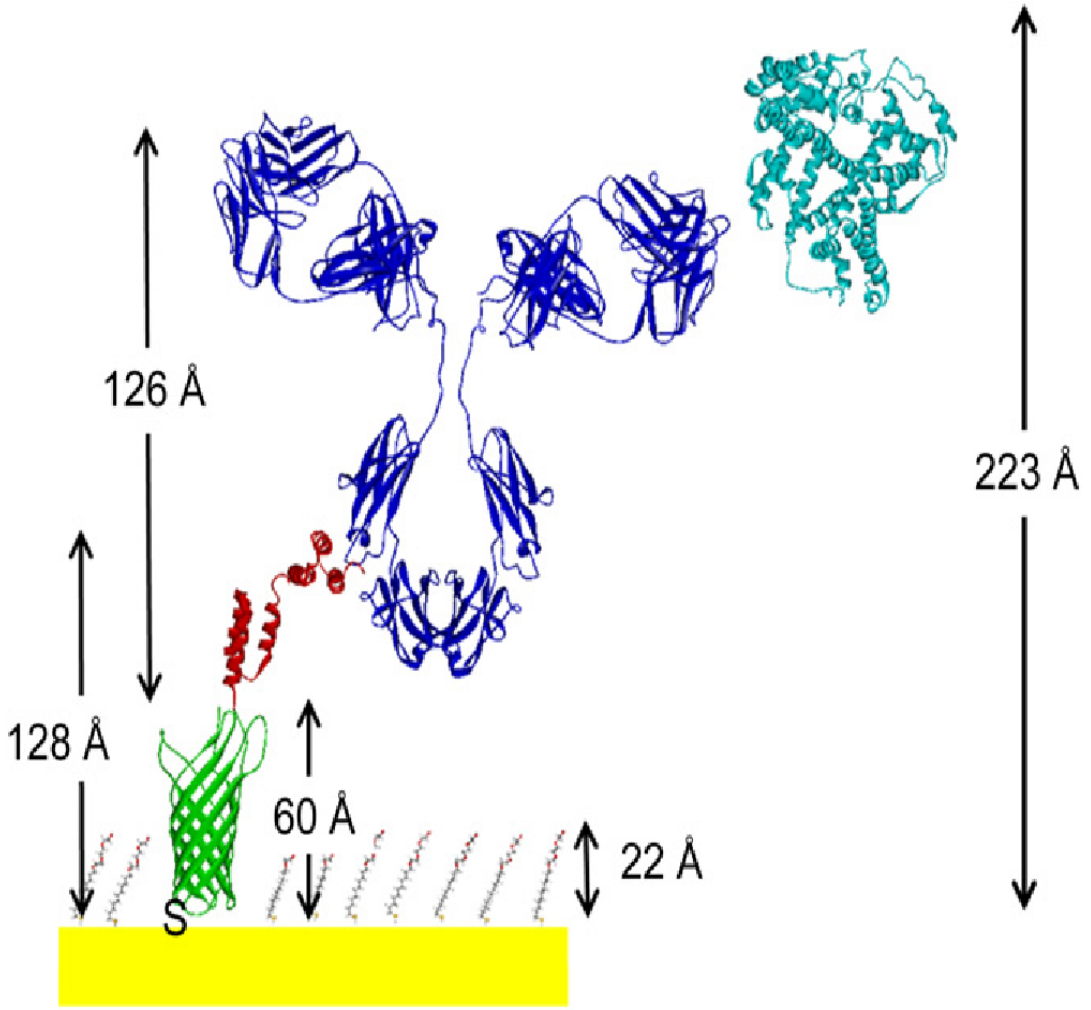

Fig. 8. A schematic of the proposed orientation of antigen bound IgG bound to gold immobilised ZZctOmpA. The ZZctOmpA molecule is immobilised to gold *via* a thiol-gold bond between the gold surface and a cysteine residue (denoted by a letter 'S') in turn four of the tOmpA domain (green β-barrel section). The tOmpA is insulated by a 22 Å layer of thioPEG. The one of the Z domains (red) of ZZctOmpA will bind IgG at its constant region leaving the variable region to bind antigen which in this case was HSA (light blue).

Part 4: Application of polarized neutrons in measurements of very small energy and momentum transfers with condensed matter

<> the precession of the neutron spin in a magnetic field can be used as an accurate measure of length from which changes in angle (momentum or wavevector direction) or neutron speed (energy or wavevector magnitude) can be determined

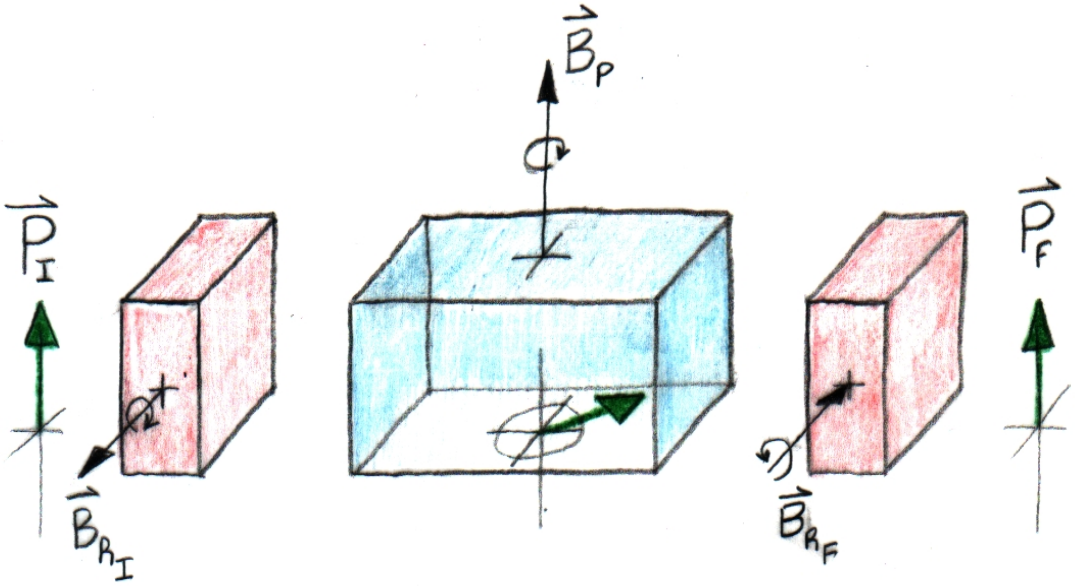

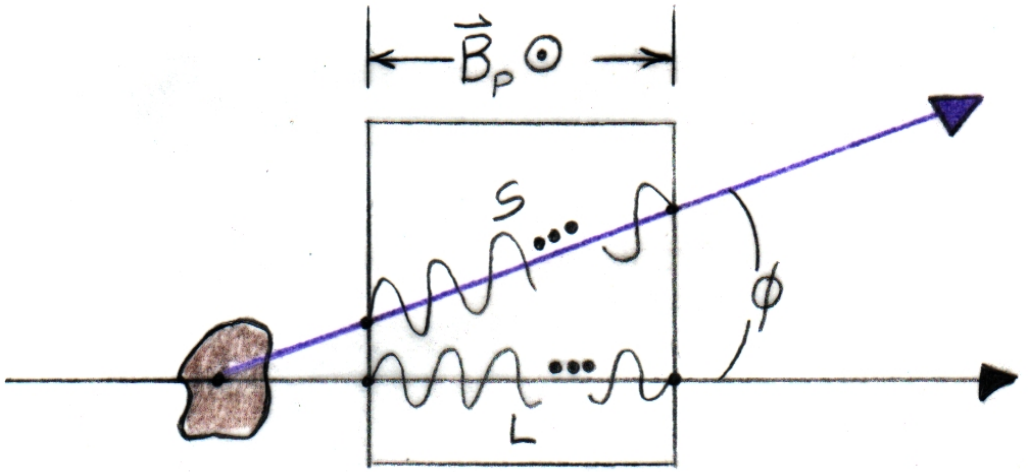

$$P_y(n) = \cos\underbrace{\left[(M_- - M_+)k_0 n\right]}_{\propto (B\lambda n)}$$

$$S\cos\phi = L$$

Imagine, in the top part of the figure, a neutron beam prepared with initial polarization **P** along the vertical axis propagating from left to right. **P** is then rotated 90 deg into the horizontal plane in the region defined by the blue box where a magnetic field is applied along the vertical z-axis. Precession of the polarization occurs in this region and the final in-plane polarization vector upon emerging from this region is projected back along the vertical axis in another 90 deg rotator device so that the final polarization component along the vertical z-axis can be determined (with a polarization analyser such as a magnetic mirror). By tuning the magnitude of the precession field for the velocity (or wavelength) of the neutron and the length L of the region, an integral number, say, of full 360 deg rotations can take place in that region. If the neutrons are made to deviate from normal incidence through the precession region by scattering from a material object to take a longer path S, then the observed change in the number of precessions can be used as a measure of the scattering angle phi via the geometry. For example, at a wavelength of 5 A, B = 1000 Gauss, and L = 1 m, approximately 3610.0 full rotations take place -- at a scattering angle of 1 deg, about 3610.5 occur along path S -- which is a phase change of 180 deg that can be accurately measured.

Neutron spin-echo labeling of angle: after work of Felcher, te Velthuis, Rekveldt, Pynn, Major and others. (Thanks to Suzanne te Velthuis for this and next figure!) Note that because the lengths of neutron trajectories through the magnetic precession region depend upon angle, so does the amount of polarization rotation. But by placing a second precession region in series with the first which is identical except for the *direction* of the applied magnetic field (which is exactly opposite), the net rotation acquired in the first region is exactly reversed in the second for each individual neutron path. Thus, the final polarization state of the beam is the same as it was initially.

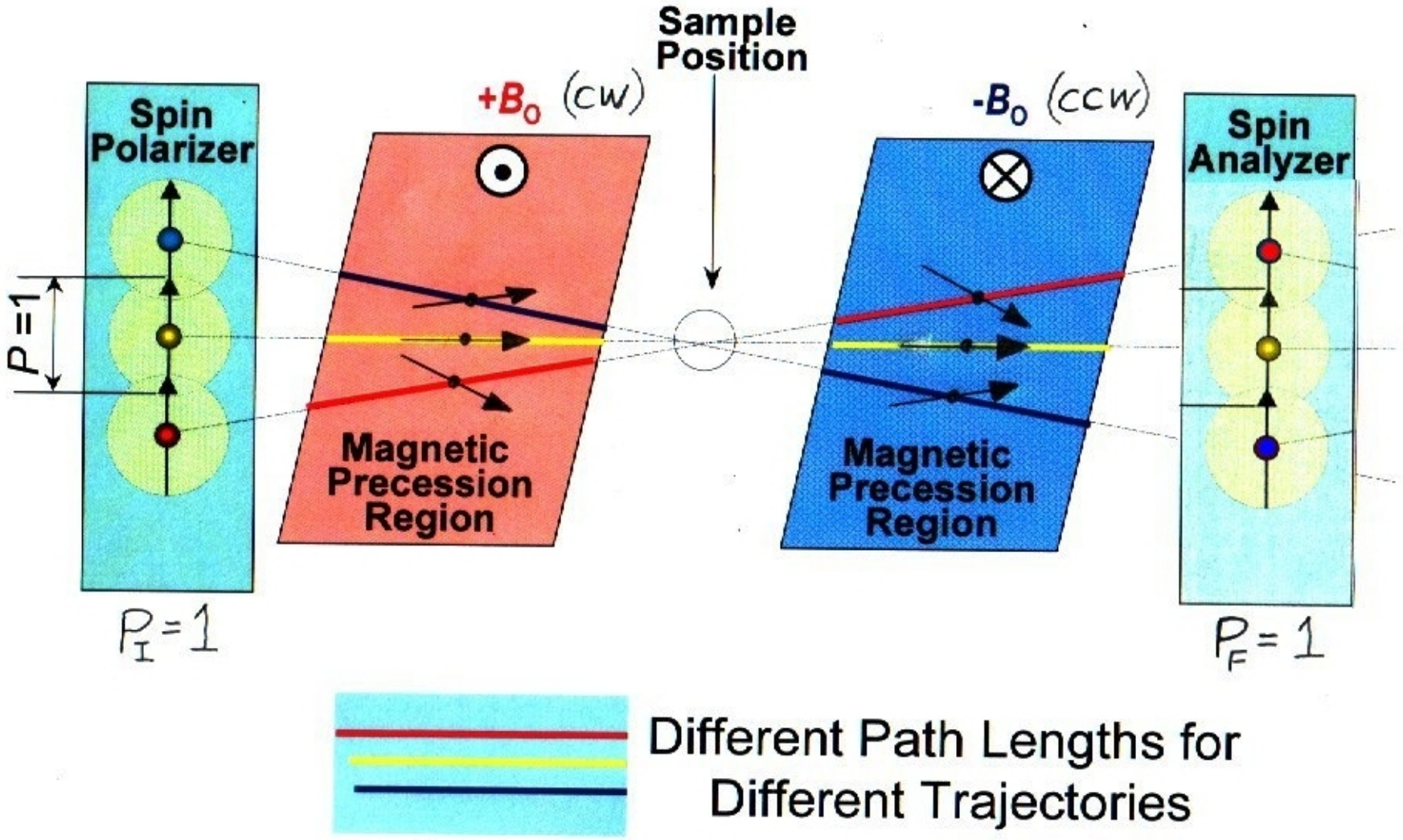

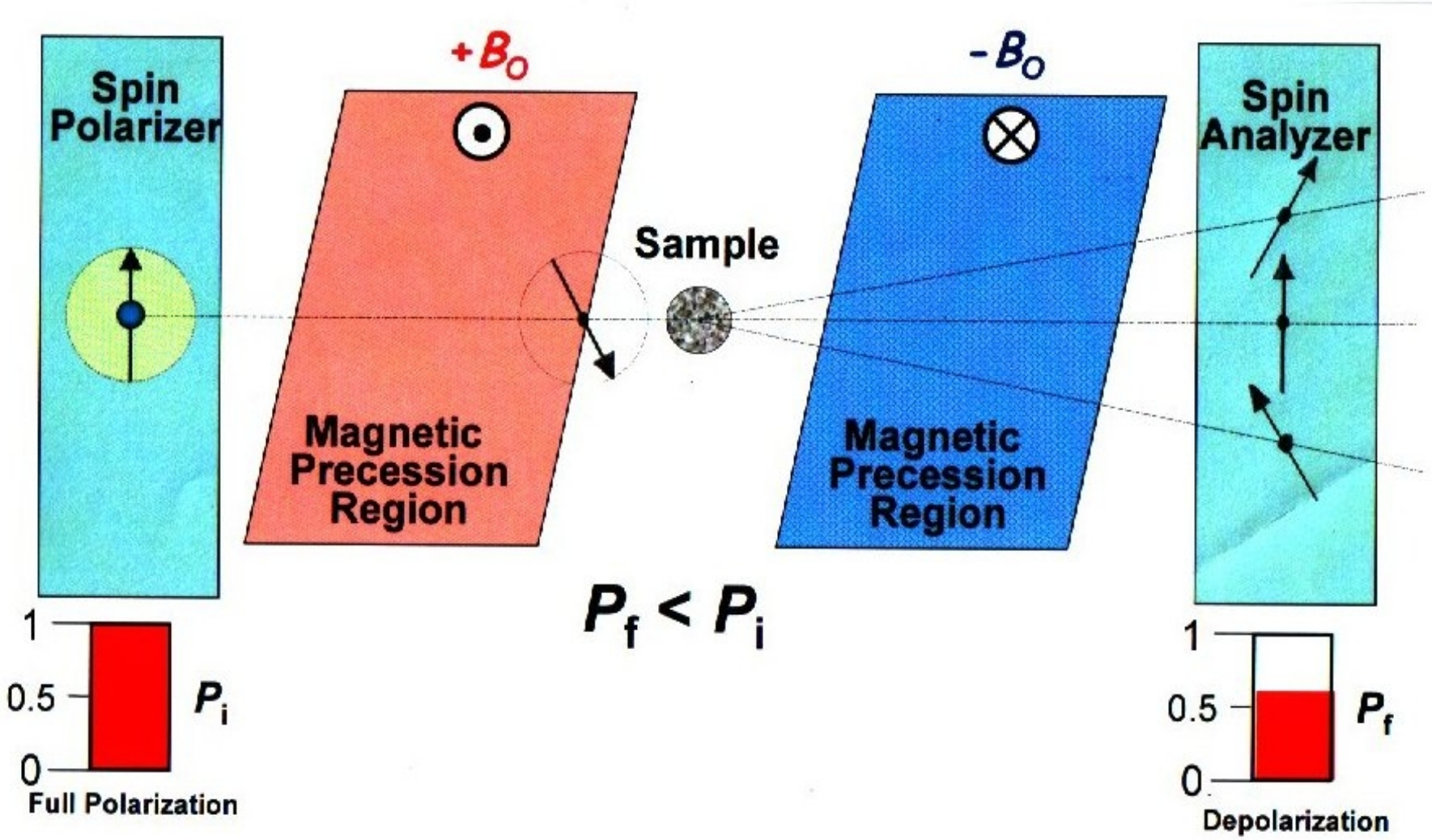

If elastic scattering at some angle from a sample placed in between the two precession regions occurs, then the net cancellation of clockwise and counterclockwise rotations of the polarization along a given trajectory no longer occurs in general and the final polarization can differ from the initial value. The “echo” condition is no longer satisfied completely.

NSE LABELLING OF ANGLE : PRECESSION FIELD GEOMETRY

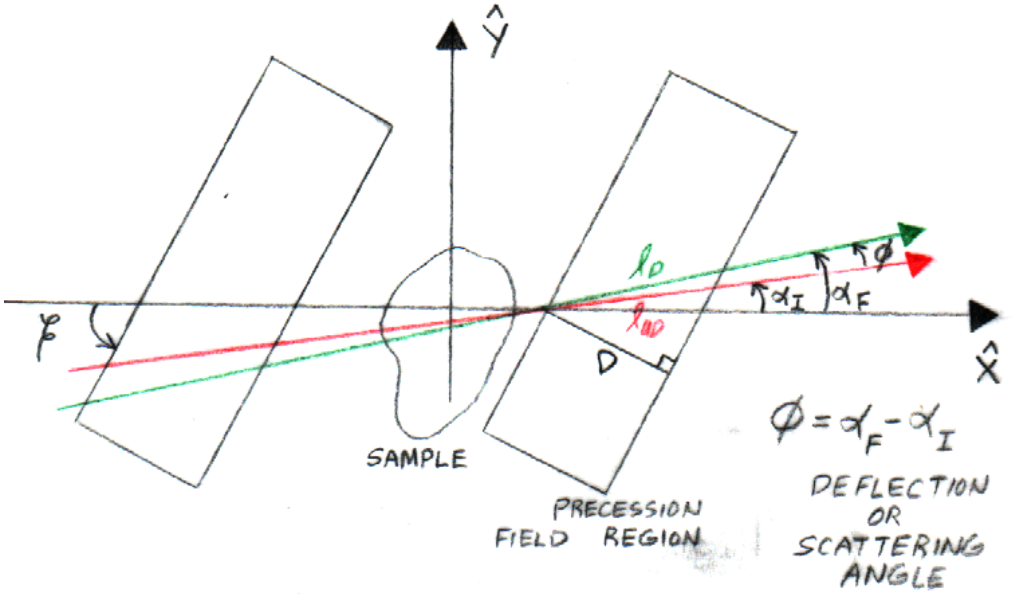

$$\ell_D \sin(\xi - \alpha_F) = D = \ell_{UD} \sin(\xi - \alpha_I)$$

PATH LENGTH DIFFERENCE $\Delta\ell = \ell_D - \ell_{UD}$

$$\Delta\ell = D\left[\frac{1}{\sin(\xi - \alpha_F)} - \frac{1}{\sin(\xi - \alpha_I)}\right]$$

AT SUFFICIENTLY SMALL ANGLES

$$\Delta\ell \simeq D\left(\frac{\cos\xi}{\sin^2\xi}\right)$$

DIFFRACTION FROM GRATING STRUCTURE ALONG Y-DIRECTION (IN PLANE)

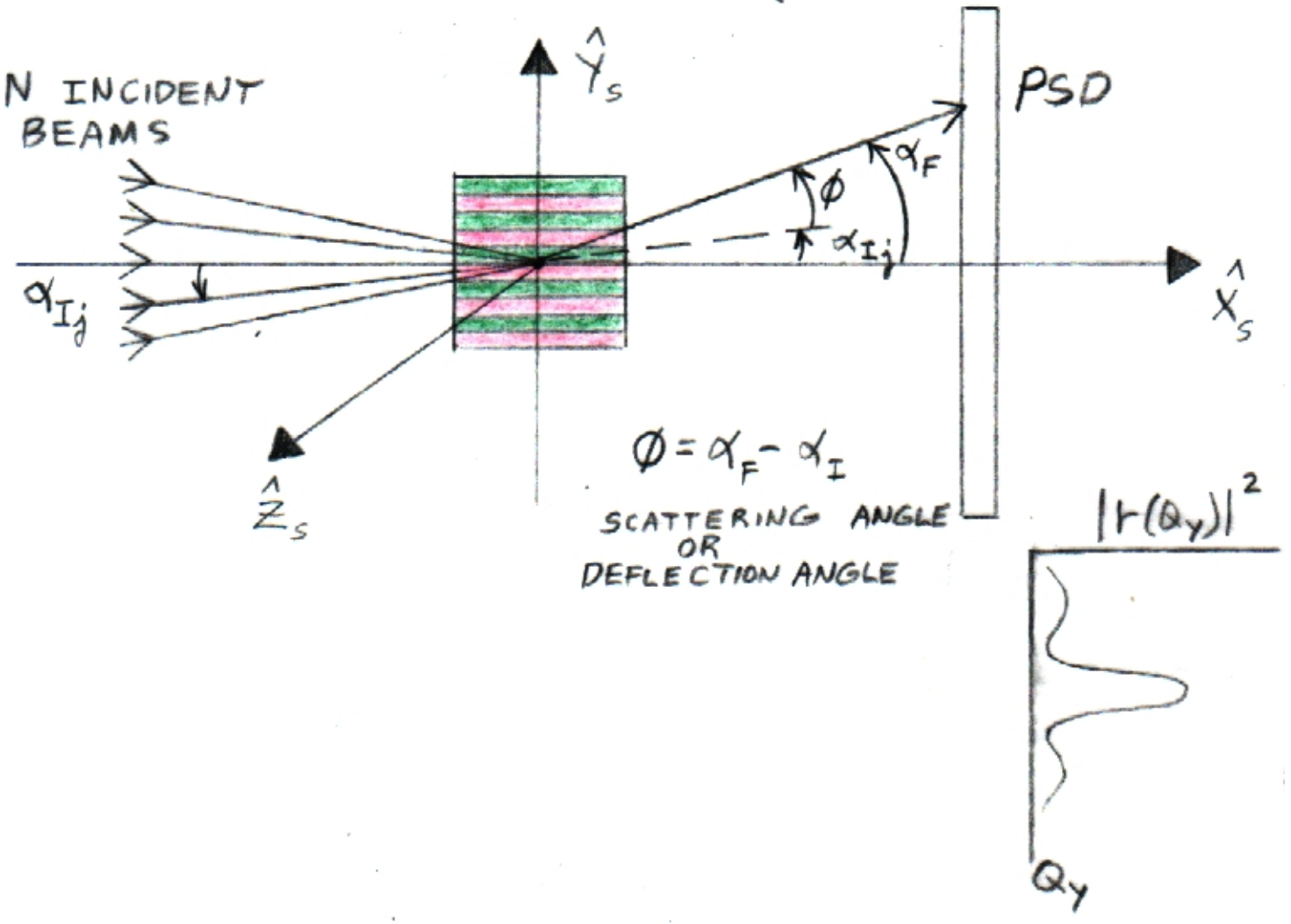

$|r|^2 \equiv$ REFLECTED INTENSITY / INCIDENT INTENSITY

DIFFRACTION FROM GRATING STRUCTURE ALONG Y-DIRECTION (IN PLANE)

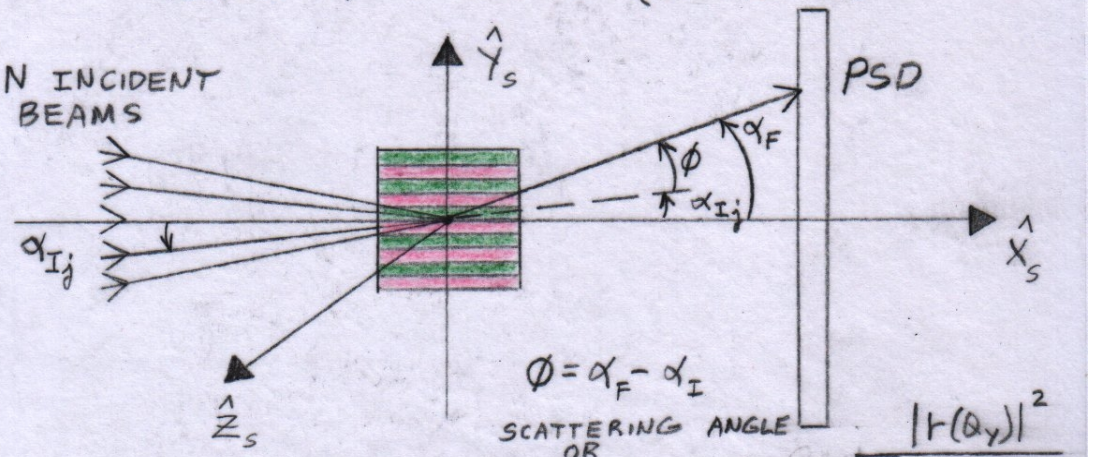

SOLVE SET OF SIMULTANEOUS EQUATIONS FOR $|r|^2$

$$\underbrace{S(\delta_i)}_{\begin{matrix} S_1 \\ S_2 \\ \vdots \\ S_N \end{matrix}} = \sum_{j=1}^{N} I_0 \underbrace{M(\delta_i, \alpha_{I_j}, \alpha_F)}_{\text{MODULATION FUNCTION}} \left| r(\alpha_F, \alpha_{I_j}) \right|^2$$

(δ_i = MODULATION PARAMETER)

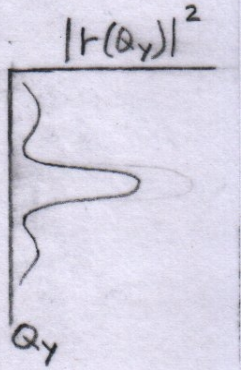

$|r|^2 \equiv \frac{\text{REFLECTED INTENSITY}}{\text{INCIDENT INTENSITY}}$

e.g., $$M = \frac{I_\pm}{I_0} = \left[\frac{1 \pm \cos\beta}{2}\right]$$

OR

$$M = P_x = \frac{I_+ - I_-}{I_+ + I_-} = \cos\beta$$

WHERE β = CONSTANT B $\Delta\ell$

AND $$\Delta\ell = \left[\frac{D(\alpha_F - \alpha_I)}{(\xi^2 - \alpha_F\xi - \alpha_I\xi + \alpha_F\alpha_I)}\right]$$

ξ = "TILT" ANGLE OF RECTANGULAR PRECESSION FIELD REGION

J. Major et al., Physica B 336 (2003) 8-15

$$Q_y \simeq k(\alpha_F - \alpha_I) \equiv k\phi$$

$$|r_{BA}(Q_y)|^2 \propto \left| \int \rho(y) e^{iQ_y y} dy \right|^2$$

$$P_x(\delta^{SE}) = \int |r(\phi)|^2 \cos(k\phi\delta^{SE}) d\phi$$

WHERE $\underbrace{\delta^{SE}}_{\text{SPIN ECHO "LENGTH"}} = \underbrace{\left[\frac{m_n \gamma_n \lambda^2}{2\pi h}\right]}_{\text{CONSTANT}} \left(\frac{B\,D}{\sin\xi} \frac{\cos\xi}{\sin\xi}\right)$

PRECESSION FIELD TILT ANGLE

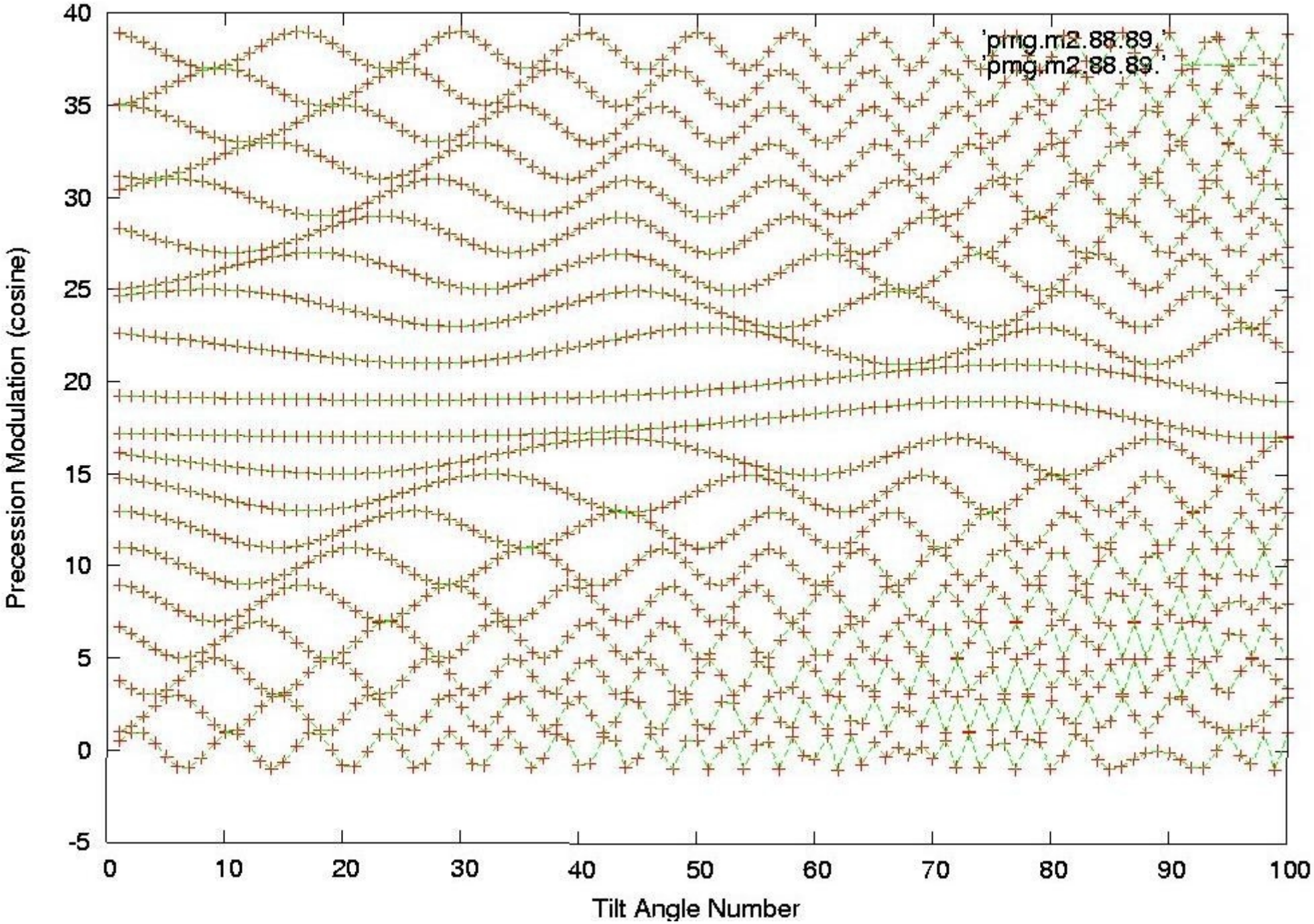
'pmg.m2.88.89.'
'pmg.m2.88.89.'
Precession Modulation (cosine)
Tilt Angle Number
40
35
30
25
20
15
10
5
0
-5
0
10
20
30
40
50
60
70
80
90
100

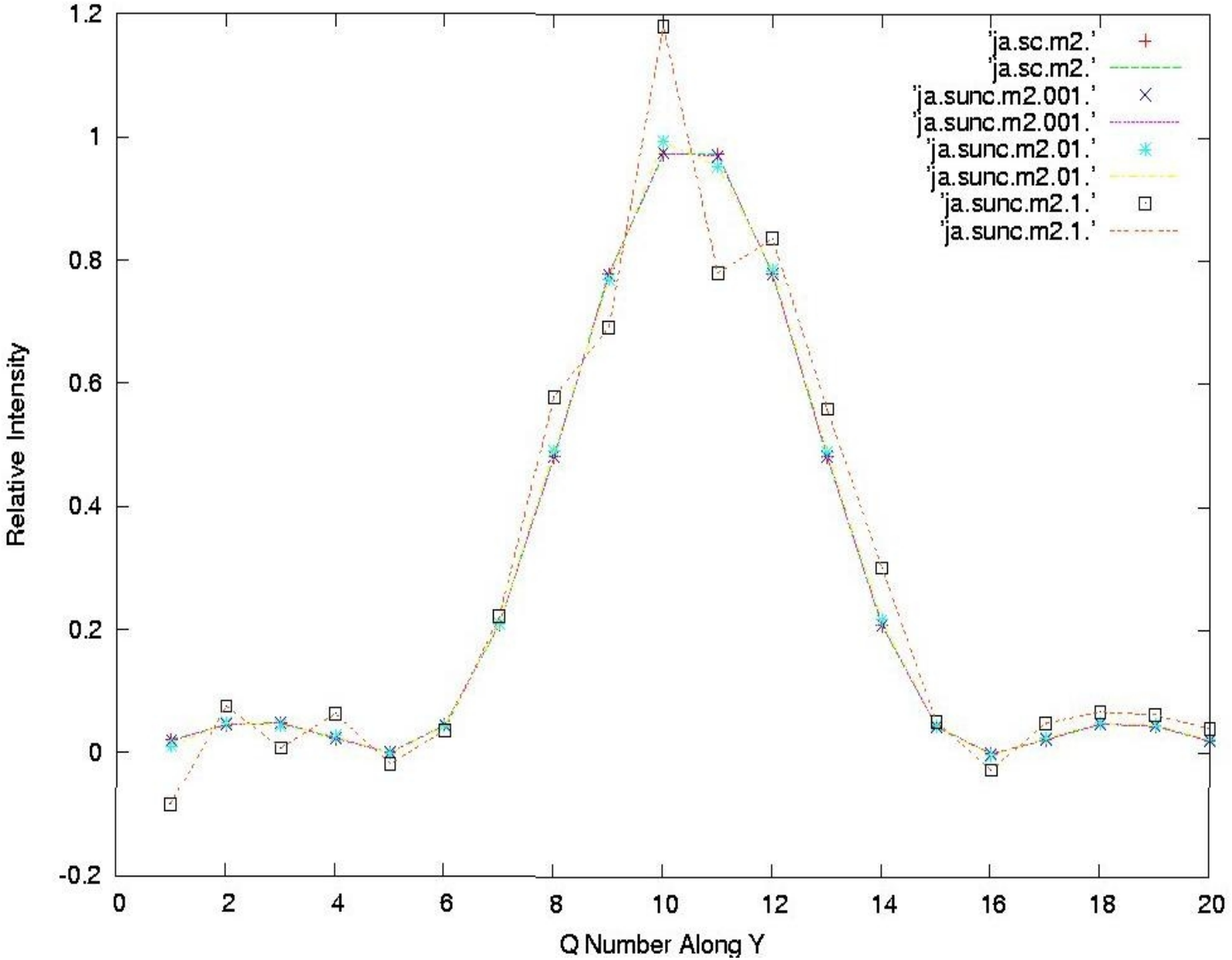

Comparison of inverted grating diffraction pattern to model where modulation of the beam was performed according to the spin-echo labeling method (blue asterisk symbols correspond to model and squares to calculated inversion).

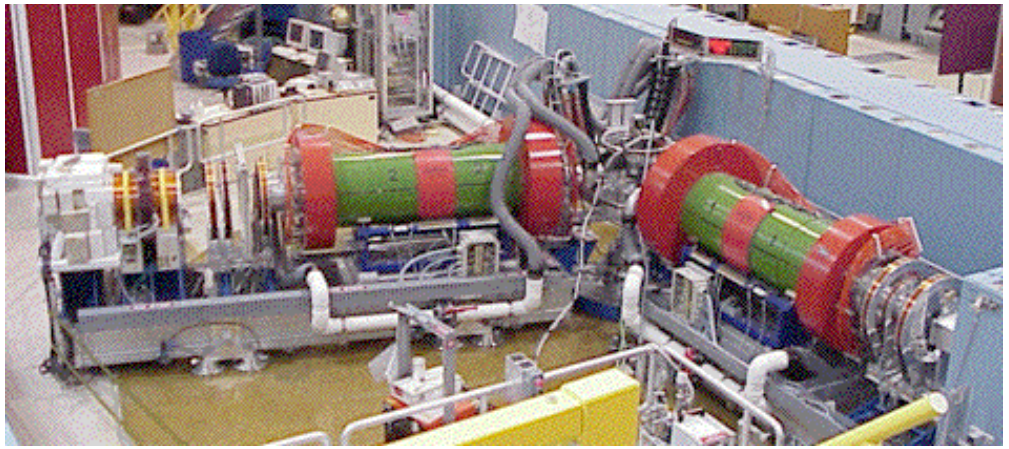

Spin Echo Spectrometer
on NG5 at the NCNR

Spin Tagging Demonstration[1]
on EVA at the ILL, France

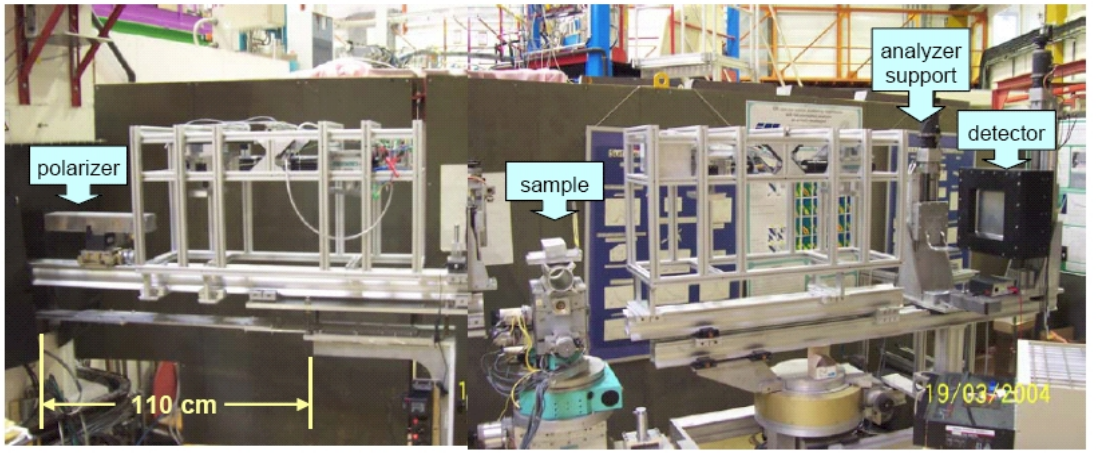

[1]J. Major, H. Dosch, G.P. Felcher, *et al*., Physica B (2003).
Also, M. Th. Rekveldt, *et al.,* Rev. Sci. Instr. (2005).
And R. Pynn, M.R. Fitzsimmons, *et al*., Rev. Sci. Instr. (2005).

“Polarized Neutron Reflectometry”, C.F.Majkrzak, K.V.O'Donovan, and N.F.Berk, Chapter 9 in *Neutron Scattering from Magnetic Materials*, Edited by T.Chatterji, (Elsevier, Amsterdam, 2006) p.397-471.

Polarized Neutrons, W. Gavin Williams, (Clarendon Press, Oxford, 1988)

www.ncnr.nist.gov -- variety of references and articles on the subject of polarized neutron scattering.

Appendices

<> X-ray magnetic scattering

<> Supermirror polarizer for neutrons

<> Polarized neutron beam corrections for efficiencies of polarizers and flippers

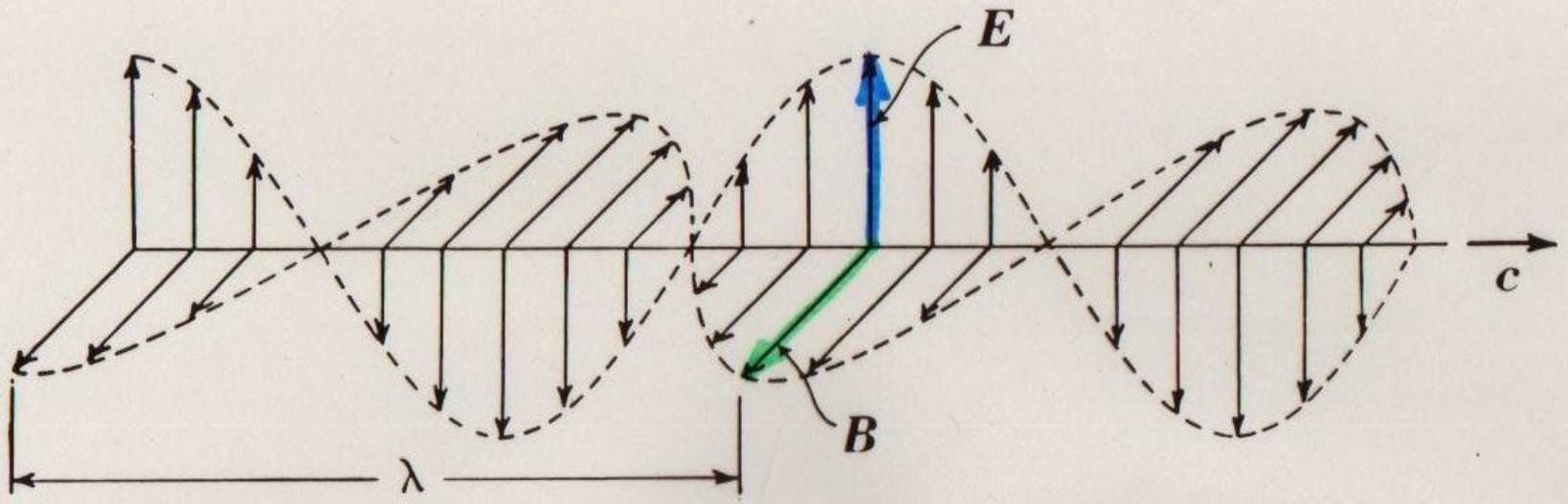

Figure 41-15. Representations of the electric and magnetic fields of a sinusoidal electromagnetic wave: (a) the field lines; (b) the sinusoidally varying amplitudes. (after Weidner & Sells, Elementary Classical Physics)

PHOTON

- ZERO MASS
- VELOCITY (IN VACUUM)

$$c_0 \cong 3 \times 10^8 \text{ m/sec}$$

- POLARIZED ELECTROMAGNETIC WAVE

Non-Resonant Magnetic X-Ray Scattering

<> X-rays interact with magnetic as well as with electronic charge distributions -- the magnetic scattering of x-rays is a relativistic effect.

<> For non-resonant x-ray scattering, $I_{MAGNETIC} / I_{CHARGE} \approx 10^{-6}$.

<> $r_{CHARGE} \alpha$ FT(charge density) x C

$r_{MAGNETIC} \alpha$ (1/2) FT(orbital density L) x A + FT(spin density S) x B

where the factors A, B, and C describe the polarization dependence of the scattering.

(For neutrons, the magnetic scattering amplitude is proportional to (L + 2S) so that the L and S contributions cannot be directly separated -- however, because the spatial extents of the magnetic densities corresponding to L and S are different, modeling and fitting allows for separation, at least in principle.)

Resonant Magnetic X-Ray Scattering

<> Resonant enhancement can be as large as 10^6.

<> Resonant magnetic scattering is element specific.

<> As an example, in Ho and at an incident x-ray energy near the L(III) absorption edge, the incident photon excites a 3p electron to the 5d unoccupied level -- under these conditions electric 2^L pole resonances are stimulated and contribute to the coherent scattering amplitude: the process can roughly be described as one in which a core electron is excited to an unoccupied level and forms a *magnetic resonance* with the *unpaired electrons* in that particular shell.

Details about magnetic x-ray scattering can be found, for instance, in the work of Doon Gibbs and colleagues on this subject (and from which the above information was obtained).

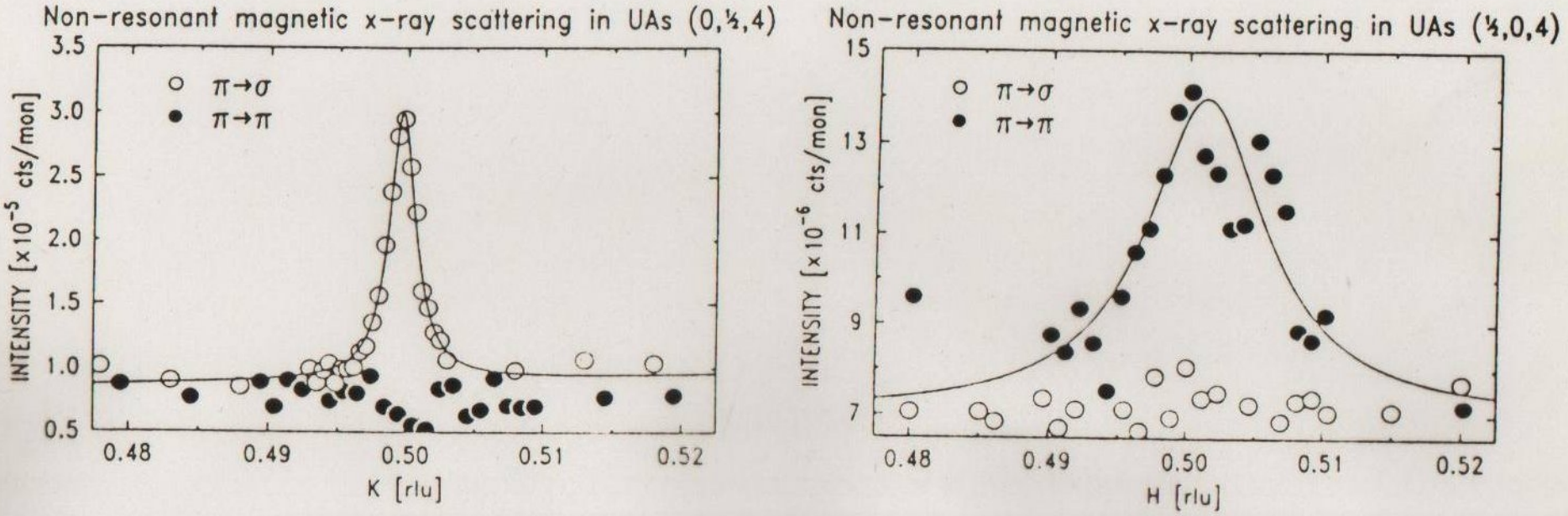

Fig. 2: Experimental results taken with different polarization (as indicated) for the satellites around the (004) charge peak in UAs. Based on Eq. (4) and our understanding of the magnetic structure (from neutrons) the structure factors are proportional to:

left hand side: $(\pi \rightarrow \pi)$ zero $(\pi \rightarrow \sigma)$ $(L + S)$

right hand side: $(\pi \rightarrow \pi)$ $(\sim 0.5L + S)$ $(\pi \rightarrow \sigma)$ $(\sim 0.1\ S)$

(AFTER G. LANDER et al.)

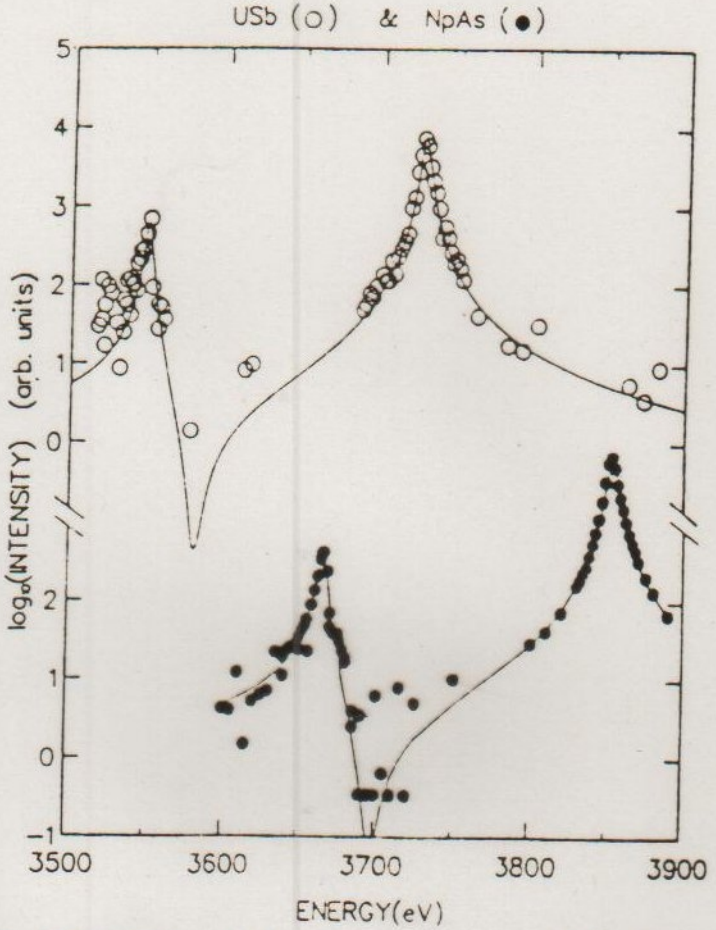

Fig. 3: Intensity of the magnetic satellite from a uranium and neptunium compound as a function of energy. The solid lines are fits to atomic resonance theory. (Taken from Ref. 24 and 25)

(D. GIBBS et al.)

(G. LANDER et al.)

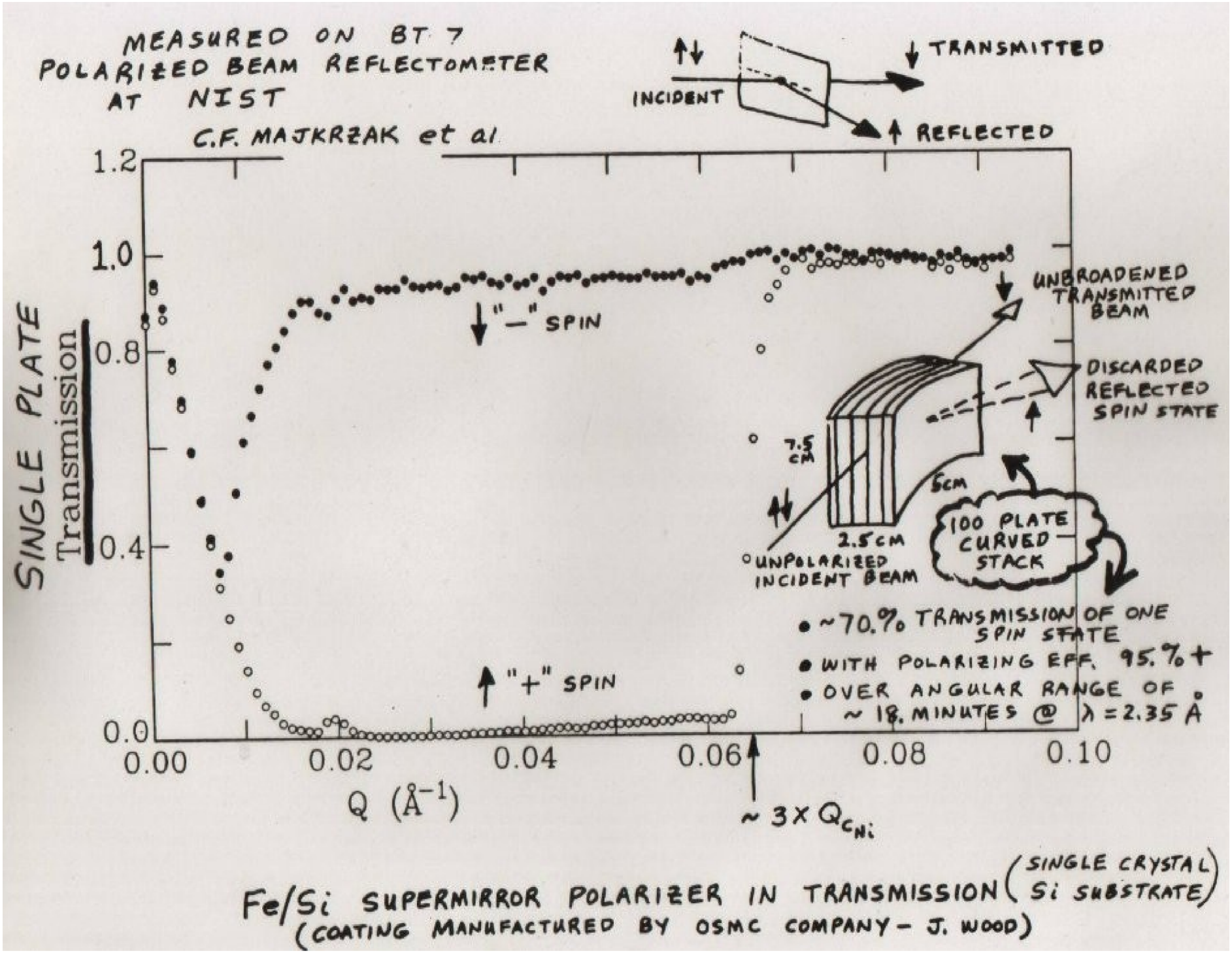

Fe/Si SUPERMIRROR POLARIZER IN TRANSMISSION (SINGLE CRYSTAL Si SUBSTRATE)
(COATING MANUFACTURED BY OSMC COMPANY – J. WOOD)

TABLE 2: POLARIZING AND FLIPPING EFFICIENCY CORRECTIONS

$\sigma_{++}, \sigma_{--}, \sigma_{+-}$, and σ_{-+} are defined as the NSF and SF reflectivities, respectively, corresponding to the sample.

$I^{off\ off}$, $I^{on\ on}$, $I^{off\ on}$, and $I^{on\ off}$ are defined as the intenisities measured with front and rear flippers respectively, in "on" (π rotation of the neutron spin) or "off" (no rotation) states.

F, R, f, and r are defined as the front and rear polarizer and front and rear flipper efficiencies, respectively.

The relationship between the intensities measured in the detector and the sample spin-dependent reflectivities are [28]

$$
\begin{aligned}
I^{off\ off}/\beta = {} & \sigma_{++}(1+F)(1+R) \\
& +\sigma_{-+}(1-F)(1+R) \\
& +\sigma_{--}(1-F)(1-R) \\
& +\sigma_{+-}(1+F)(1-R)
\end{aligned}
\qquad
\begin{aligned}
I^{on\ off}/\beta = {} & \sigma_{++}(1+R)[1+F(1-2f)] \\
& +\sigma_{-+}(1+R)[1-F(1-2f)] \\
& +\sigma_{--}(1-R)[1-F(1-2f)] \\
& +\sigma_{+-}(1-R)[1+F(1-2f)]
\end{aligned}
$$

$$
\begin{aligned}
I^{off\ on}/\beta = {} & \sigma_{++}(1+F)[1+R(1-2r)] \\
& +\sigma_{-+}(1-F)[1+R(1-2r)] \\
& +\sigma_{--}(1-F)[1-R(1-2r)] \\
& +\sigma_{+-}(1+F)[1-R(1-2r)]
\end{aligned}
\qquad
\begin{aligned}
I^{on\ on}/\beta = {} & \sigma_{++}[1+F(1-2f)][1+R(1-2r)] \\
& +\sigma_{-+}[1-F(1-2f)][1+R(1-2r)] \\
& +\sigma_{--}[1-F(1-2f)][1-R(1-2r)] \\
& +\sigma_{+-}[1+F(1-2f)][1-R(1-2r)]
\end{aligned}
$$

The spin-dependent reflectivities can be solved for from the measured intensities if the instrumental polarizing and flipping efficiencies and the constant β are determined.

The constant β is given by

$$2\beta = \frac{I_{NS}^{on\ on} I_{NS}^{off\ off} - I_{NS}^{on\ off} I_{NS}^{off\ on}}{I_{NS}^{on\ on} + I_{NS}^{off\ off} - I_{NS}^{on\ off} - I_{NS}^{off\ on}} \equiv \alpha$$

where the subscript "NS" signifies measurements at zero scattering angle with "no sample" in place. Also,

$$
\begin{aligned}
I_{NS}^{off\ off}/\alpha &= FR+1 \\
I_{NS}^{on\ off}/\alpha &= FR(1-2f)+1 \\
I_{NS}^{off\ on}/\alpha &= FR(1-2r)+1
\end{aligned}
$$

so that f, r, and the product F R can be determined.

If the sample is replaced with a "reference sample" (RS) which has $\sigma_{++} \neq \sigma_{--}$ and $\sigma_{+-} = \sigma_{-+} = 0$ (σ_{++} and σ_{--} need not be known), then F and R can be individually determined.

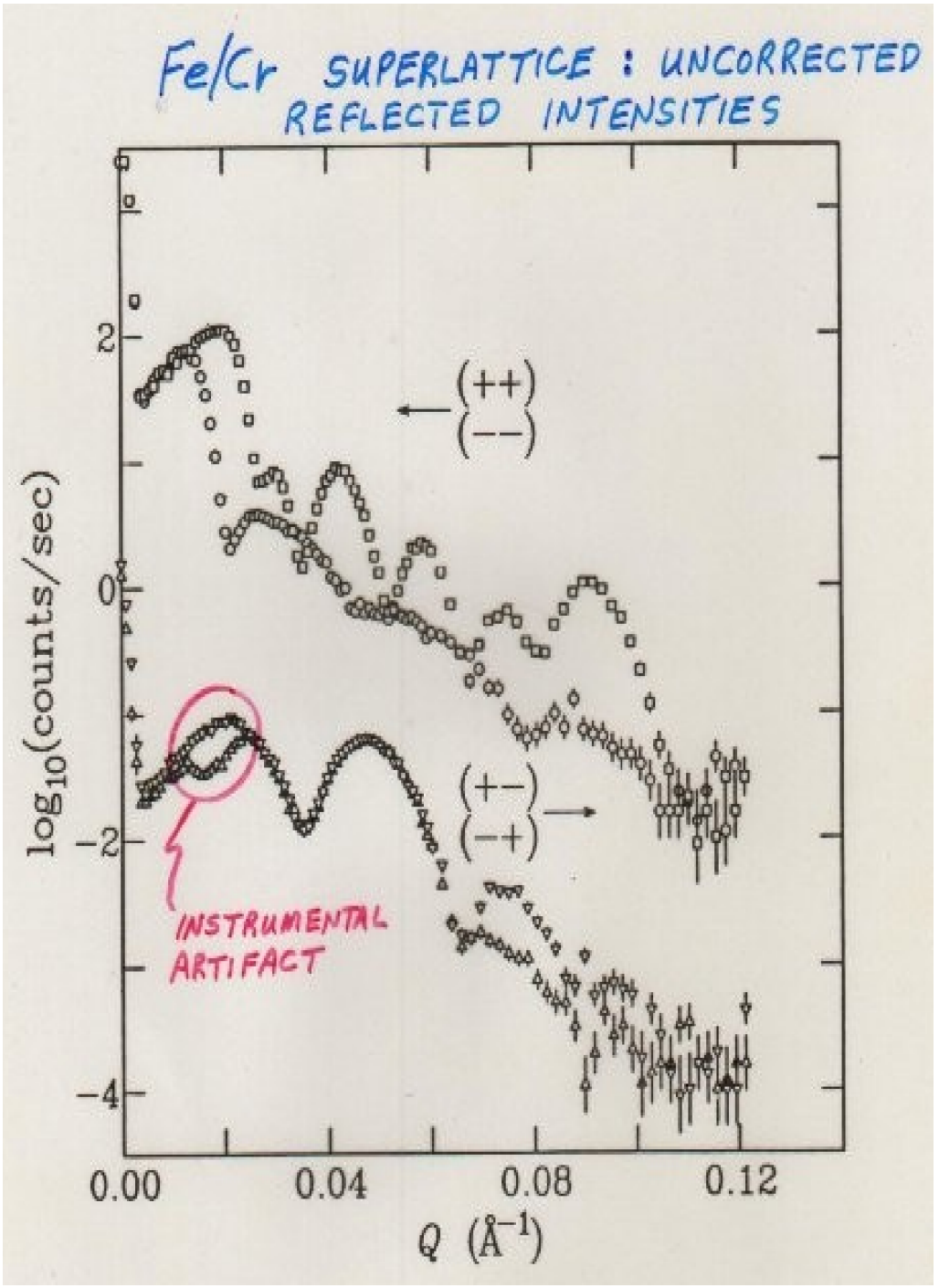
Fe/Cr SUPERLATTICE : UNCORRECTED
REFLECTED INTENSITIES
log10(counts/sec)
2
0
−2
−4
(++)
(−−)
(+−)
(−+)
INSTRUMENTAL
ARTIFACT
0.00
0.04
0.08
0.12
Q (Å−1)

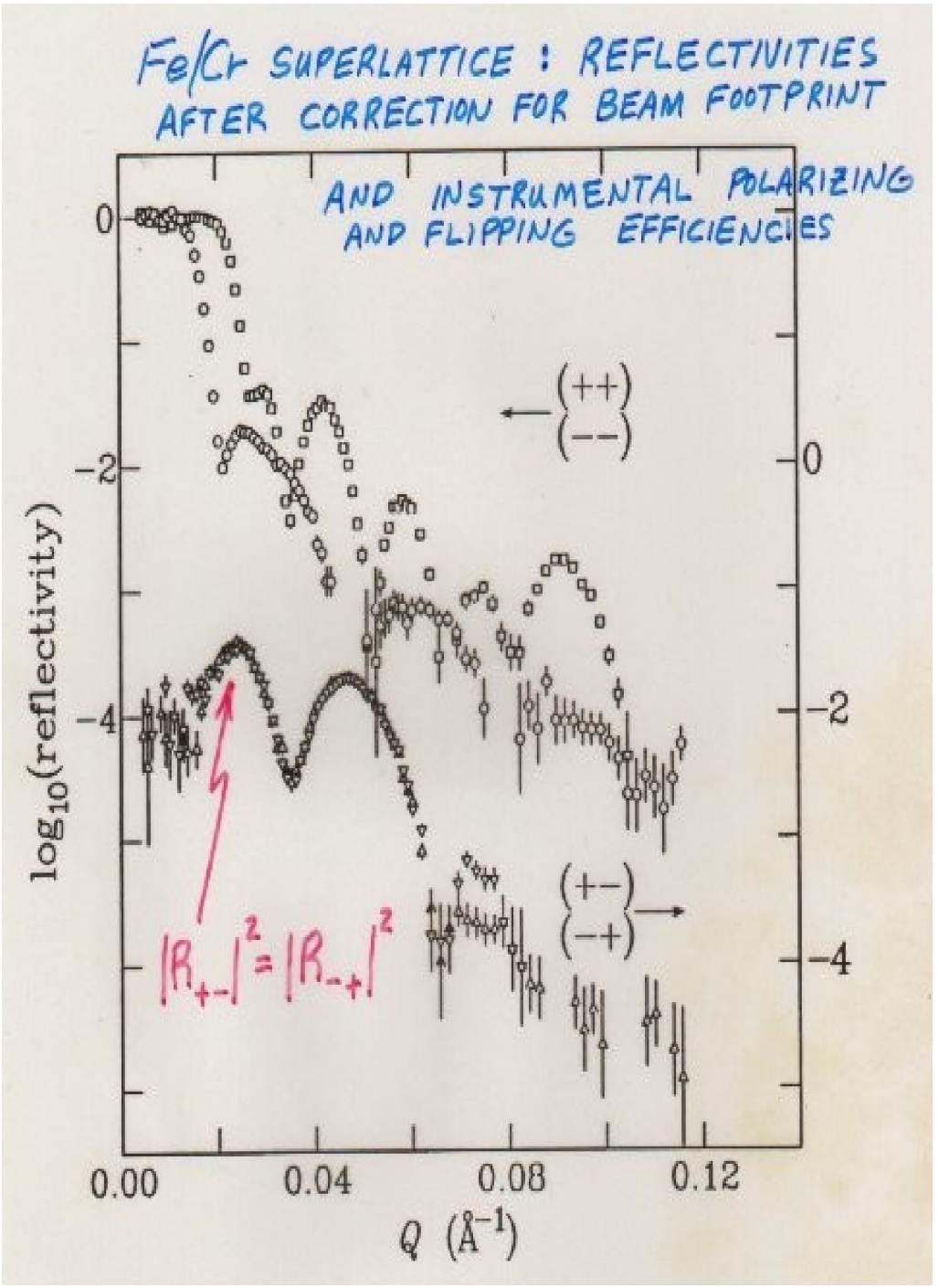
Fe/Cr SUPERLATTICE : REFLECTIVITIES
AFTER CORRECTION FOR BEAM FOOTPRINT
AND INSTRUMENTAL POLARIZING
AND FLIPPING EFFICIENCIES
log10(reflectivity)
0
−2
−4
(++)
(−−)
(+−)
(−+)
|R+−|2 = |R−+|2
0.00
0.04
0.08
0.12
Q (Å−1)